

1 **Naturally enhanced neutralizing breadth to SARS-CoV-2 after one year**

2

3

4 Zijun Wang<sup>1,\*</sup>, Frauke Muecksch<sup>2,\*</sup>, Dennis Schaefer-Babajew<sup>1,\*</sup>, Shlomo Finkin<sup>1,\*</sup>, Charlotte

5 Viant<sup>1,\*</sup>, Christian Gaebler<sup>1,\*</sup>, Hans-Heinrich Hoffmann<sup>3</sup>, Christopher O. Barnes<sup>4</sup>, Melissa

6 Cipolla<sup>1</sup>, Victor Ramos<sup>1</sup>, Thiago Y. Oliveira<sup>1</sup>, Alice Cho<sup>1</sup>, Fabian Schmidt<sup>2</sup>, Justin da Silva<sup>2</sup>, Eva

7 Bednarski<sup>2</sup>, Lauren Aguado<sup>3</sup>, Jim Yee<sup>5</sup>, Mridushi Daga<sup>1</sup>, Martina Turroja<sup>1</sup>, Katrina G. Millard<sup>1</sup>,

8 Mila Jankovic<sup>1</sup>, Anna Gazumyan<sup>1,6</sup>, Zhen Zhao<sup>5</sup>, Charles M. Rice<sup>3</sup>, Paul D. Bieniasz<sup>2,6</sup>, Marina

9 Caskey<sup>1</sup>, Theodora Hatziioannou<sup>2</sup>, Michel C. Nussenzweig<sup>1,6</sup>

10

11

12

13 <sup>1</sup>Laboratory of Molecular Immunology, The Rockefeller University, New York, NY 10065, USA

14 <sup>2</sup>Laboratory of Retrovirology, The Rockefeller University, New York, NY 10065, USA

15 <sup>3</sup>Laboratory of Virology and Infectious Disease, The Rockefeller University, New York, NY,

16 10065, USA.

17 <sup>4</sup>Division of Biology and Biological Engineering, California Institute of Technology, Pasadena,

18 CA, USA.

19 <sup>5</sup>Department of Pathology and Laboratory Medicine, Weill Cornell Medicine, New York, NY,

20 10065, USA

21 <sup>6</sup>Howard Hughes Medical Institute

22

23 \*equal contribution

24 Address correspondence to: Paul D. Bieniasz, [pbieniasz@rockefeller.edu](mailto:pbieniasz@rockefeller.edu); Marina Caskey,  
25 [mcaskey@rockefeller.edu](mailto:mcaskey@rockefeller.edu); Theodora Hatziiioannou, [thatziio@rockefeller.edu](mailto:thatziio@rockefeller.edu); or Michel C.  
26 Nussenzweig, [nussen@rockefeller.edu](mailto:nussen@rockefeller.edu).

27

28

29 **Over one year after its inception, the coronavirus disease-2019 (COVID-19) pandemic**  
30 **caused by severe acute respiratory syndrome coronavirus-2 (SARS-CoV-2) remains**  
31 **difficult to control despite the availability of several excellent vaccines. Progress in**  
32 **controlling the pandemic is slowed by the emergence of variants that appear to be more**  
33 **transmissible and more resistant to antibodies<sup>1,2</sup>. Here we report on a cohort of 63 COVID-**  
34 **19-convalescent individuals assessed at 1.3, 6.2 and 12 months after infection, 41% of**  
35 **whom also received mRNA vaccines<sup>3,4</sup>. In the absence of vaccination antibody reactivity to**  
36 **the receptor binding domain (RBD) of SARS-CoV-2, neutralizing activity and the number**  
37 **of RBD-specific memory B cells remain relatively stable from 6 to 12 months. Vaccination**  
38 **increases all components of the humoral response, and as expected, results in serum**  
39 **neutralizing activities against variants of concern that are comparable to or greater than**  
40 **neutralizing activity against the original Wuhan Hu-1 achieved by vaccination of naïve**  
41 **individuals<sup>2,5-8</sup>. The mechanism underlying these broad-based responses involves ongoing**  
42 **antibody somatic mutation, memory B cell clonal turnover, and development of**  
43 **monoclonal antibodies that are exceptionally resistant to SARS-CoV-2 RBD mutations,**  
44 **including those found in variants of concern<sup>4,9</sup>. In addition, B cell clones expressing broad**  
45 **and potent antibodies are selectively retained in the repertoire over time and expand**  
46 **dramatically after vaccination. The data suggest that immunity in convalescent individuals**

47 **will be very long lasting and that convalescent individuals who receive available mRNA**  
48 **vaccines will produce antibodies and memory B cells that should be protective against**  
49 **circulating SARS-CoV-2 variants.**

50

51 We initially characterized immune responses to SARS-CoV-2 in a cohort of convalescent  
52 individuals 1.3 and 6.2 months after infection<sup>3,4</sup>. Between February 8 and March 26, 2021, 63  
53 participants between the ages of 26 and 73 years old (median 47 years) returned for a 12-month  
54 follow-up visit. Among those, 26 (41%) had received at least one dose of either the Moderna  
55 (mRNA-1273) or Pfizer-BioNTech (BNT162b2) vaccines, on average 40 days (range 2-82 days)  
56 before their study visit and 311 days (range 272-373 days) after onset of acute illness  
57 (Supplementary Table 1). Participants were almost evenly split between sexes (43% female)  
58 and of the individuals that returned for a 12-month follow-up, only 10% had been hospitalized  
59 and the remainder had experienced relatively mild initial infections. Only 14% of the individuals  
60 reported persistent long-term symptoms after 12 months, reduced from 44% at the 6-month time  
61 point<sup>4</sup>. Symptom persistence was not associated with the duration and severity of acute disease  
62 or with vaccination status (Extended Data Fig. 1 a-c). All participants tested negative for active  
63 infection at the 12-month time point as measured by a saliva-based PCR assay<sup>4</sup>. The  
64 demographics and clinical characteristics of the participants are shown in Supplementary Tables  
65 1 and 2.

66

### 67 **Plasma SARS-CoV-2 Antibody Reactivity**

68 Antibody reactivity in plasma to the RBD and nucleoprotein (N) were measured by enzyme-  
69 linked immunosorbent assay (ELISA)<sup>3</sup>. We limited our analysis to RBD because plasma anti-

70 RBD antibodies are strongly correlated with neutralizing activity<sup>3,10-12</sup>. Convalescent  
71 participants who had not been vaccinated maintained most of their anti-RBD IgM (103%), IgG  
72 (82%), and IgA (72%) titers between 6 and 12 months (Fig. 1a and Extended Data Fig. 2a-k).  
73 Consistent with previous reports<sup>5-8</sup>, vaccination increased the anti-RBD plasma antibody levels,  
74 with IgG titers increasing by nearly 30-fold compared to unvaccinated individuals (Fig. 1a right).  
75 The 2 individuals who did not show an increase had been vaccinated only 2 days before sample  
76 collection. In contrast to anti-RBD antibody titers that were relatively stable, anti-N antibody  
77 titers decreased significantly between 6 and 12 months in this assay irrespective of vaccination  
78 (Fig. 1b and Extended Data Fig. 2l-n).

79

80 Plasma neutralizing activity in 63 participants was measured using an HIV-1 pseudotyped with  
81 the SARS-CoV-2 spike protein<sup>3,4,13</sup> (Fig. 1c-d and Extended Data Fig. 2o). Twelve-months after  
82 infection, the geometric mean half-maximal neutralizing titer (NT<sub>50</sub>) for the 37 individuals that  
83 had not been vaccinated was 75, which was not significantly different from the same individuals  
84 at 6.2 months (Fig. 1c). In contrast, the vaccinated individuals showed a geometric mean NT<sub>50</sub> of  
85 3,684, which was nearly 50-fold greater than unvaccinated individuals and slightly better  
86 compared to the 30-fold increase in anti-RBD IgG antibodies (Fig. 1a, c, and d). Neutralizing  
87 activity was directly correlated with IgG anti-RBD (Extended Data Fig.2p) but not with anti-N  
88 titers (Extended Data Fig.2r). We conclude that neutralizing titers remain relatively unchanged  
89 between 6 to 12 months after SARS-CoV-2 infection, and that vaccination further boosts this  
90 activity by nearly 50-fold.

91

92 To determine the neutralizing activity against circulating variants of concern/interest, we  
93 performed neutralization assays on HIV-1 virus pseudotyped with the S protein of the following  
94 SARS-CoV-2 variants of concern/interest: B.1.1.7, B.1.351, B.1.526 and P.1<sup>1,14,15</sup>. Twelve-  
95 months after infection neutralizing activity against the variants was generally lower than against  
96 wild-type SARS-CoV-2 virus in the same assay with the greatest loss of activity against B.1.351  
97 (Fig. 1e). After vaccination the geometric mean NT<sub>50</sub> rose to 11,493, 48,341, 22,109 and 26,553  
98 against B.1.351, B.1.1.7, B.1.526 and P.1, respectively. These titers are an order of magnitude  
99 higher than the neutralizing titers we and others have reported against the wild-type SARS-CoV-  
100 2 at the peak of the initial response in infected individuals and in naïve individuals receiving both  
101 doses of mRNA vaccines (Fig. 1d and<sup>2-8</sup>). Similar results were also obtained using authentic  
102 SARS-CoV-2 WA1/2020 and B.1.351 (Extended Data Fig.2s).

103

#### 104 **Memory B cells**

105 The memory B cell compartment serves as an immune reservoir that contains a diverse collection  
106 of antibodies<sup>16,17</sup>. Although antibodies to the N-terminal domain and other parts of S can also be  
107 neutralizing, we limited our analysis to memory B cells that produce anti-RBD antibodies  
108 because they are the most numerous and potent<sup>18,19</sup>. To enumerate RBD-specific memory B  
109 cells, we performed flow cytometry using a biotin-labeled RBD<sup>3</sup> (Fig. 2a and Extended Data Fig.  
110 3a and b). In the absence of vaccination, the number of RBD specific memory B cells present at  
111 12 months was only 1.35-fold lower than the earlier timepoint (p= 0.027, Fig. 2a). In contrast  
112 and consistent with previous reports<sup>5,8,20</sup>, convalescent individuals that received mRNA vaccines  
113 showed an average 8.6-fold increase in the number of circulating RBD specific memory B cells  
114 (Fig. 2a). B cells expressing antibodies that bound to both wild-type and K417N/E484K/N501Y

115 mutant RBDs were also enumerated by flow cytometry (Extended Data Fig. 3c). The number of  
116 variant RBD cross-reactive B cells was directly proportional to but 1.6 to 3.2-fold lower than  
117 wild-type RBD binding B cells (Fig. 2a).

118

119 The memory B cell compartment accumulates mutations and undergoes clonal evolution over the  
120 initial 6 months after infection<sup>4,9,21,22</sup>. To determine whether the memory compartment continues  
121 to evolve between 6 and 12 months, we obtained 1105 paired antibody heavy and light chain  
122 sequences from 10 individuals that were also assayed at the earlier time points, 6 of which were  
123 vaccinated (Fig. 2b, Extended Data Fig 3d, Supplementary Table 3). There were few significant  
124 differences among the expressed IGHV and IGLV genes between vaccinated and un-vaccinated  
125 groups, or between the 1.3-, 6-month and 1 year time points (Extended Data Fig 4a-c)<sup>3,4</sup>. *IGHV3-*  
126 *30* and *IGHV3-53* remained over-represented irrespective of vaccination<sup>10,18</sup>(Extended Data Fig  
127 4a).

128

129 All individuals assayed at 12 months showed expanded clones of RBD-binding memory cells  
130 that expressed closely related IGHV and IGLV genes (Fig.2b, Extended Data Fig 3d and e). The  
131 relative fraction of cells belonging to these clones varied from 7-54% of the repertoire with no  
132 significant difference between vaccinated and non-vaccinated groups. The overall clonal  
133 composition differed between 6 and 12 months in all individuals suggesting ongoing clonal  
134 evolution (Fig. 2b and Extended Data Fig 3d). Among the 89 clones found after 12 months, 61%  
135 were not previously detected and 39% were present at one of the earlier time points (Fig. 2b and  
136 Extended Data Fig 3d). In vaccinated individuals the increase in size of the memory  
137 compartment was paralleled by an increase in the absolute number of B cells representing all

138 persistent clones (Extended Data Fig 5a). Thus, RBD specific memory B cell clones were re-  
139 expanded upon vaccination in all 6 convalescent individuals examined (Fig. 2b and Extended  
140 Data Fig 3d and Extended Data Fig 5a).

141

142 Somatic hypermutation of antibody genes continued between 6 and 12 months after infection  
143 (Fig. 2c). Slightly higher levels of mutation were found in individuals who had not been  
144 vaccinated compared to vaccinated individuals possibly due to recruitment of newly-formed  
145 memory cells into the expanded memory compartment of the vaccinated individuals (Fig. 2c,  
146 Extended Data Fig 5b). There was no significant difference in mutation between conserved and  
147 newly arising clones at the 12-month time point in vaccinated individuals (Extended Data Fig  
148 5c). Moreover, phylogenetic analysis revealed that sequences found at 6 and 12 months were  
149 intermingled and similarly distant from their unmutated common ancestors (Extended Data Fig  
150 6). We conclude that clonal re-expansion of memory cells in response to vaccination is not  
151 associated with additional accumulation of large numbers of somatic mutations as might be  
152 expected if the clones were re-entering and proliferating in germinal centers.

153

### 154 **Neutralizing Activity of Monoclonal Antibodies**

155 To determine whether the antibodies obtained from memory B cells 12 months after infection  
156 bind to RBD we performed ELISAs (Fig.3a). 174 antibodies were tested by ELISA including: 1.  
157 53 that were randomly selected from those that appeared only once and only after 1 year; 2. 91  
158 that appeared as expanded clones or singlets at more than one time point; 3. 30 representatives of  
159 newly arising expanded clones (Supplementary Tables 4 and 5). Among the 174 antibodies  
160 tested, 173 bound to RBD indicating that the flow cytometry method used to identify B cells

161 expressing anti-RBD antibodies was efficient (Supplementary Tables 4 and 5). The geometric  
162 mean ELISA half-maximal concentration ( $EC_{50}$ ) of the antibodies obtained after 12 months was  
163 2.6 ng/ml, which was significantly lower than at 6 months irrespective of vaccination and  
164 suggestive of an increase in affinity (Fig. 3a, Extended data Fig. 7 a and b and Supplementary  
165 Tables 4 and 5). Consistent with this observation there was an overall increase in the apparent  
166 avidity of plasma antibodies between 1.3 and 12 months <sup>3,4</sup>( $p < 0.0001$ , Extended data Fig. 7c).

167  
168 All 174 RBD binding antibodies obtained from the 12-month time point were tested for  
169 neutralizing activity in a SARS-CoV-2 pseudotype neutralization assay. When compared to the  
170 earlier time points from the same individuals, the geometric mean half maximal inhibitory  
171 concentration ( $IC_{50}$ ) improved from 171 ng/mL (1.3 months) to 116 ng/mL (6 months) to 79  
172 ng/mL (12 months), with no significant difference between vaccinated and non-vaccinated  
173 individuals (Fig. 3b and Extended data Fig. 7d, Supplementary Table 4). The increased potency  
174 was especially evident in the antibodies expressed by expanded clones of B cells that were  
175 conserved for the entire observation period irrespective of vaccination ( $p = 0.014$ , Fig. 3b right,  
176 Extended Data Fig 7e-h and Supplementary Table 5). The overall increase in neutralizing  
177 activity among conserved clones was due to accumulation of clones expressing antibodies with  
178 potent neutralizing activity and simultaneous loss of clones expressing antibodies with no  
179 measurable activity ( $p = 0.028$ , Fig 3b right pie charts). Consistent with this observation,  
180 antibodies obtained from clonally expanded B cells after 12 months were more potent than  
181 antibodies obtained from unique B cells at the same time point ( $p = 0.029$ , Fig 3b).

182

183 **Epitopes and Breadth of Neutralization**



184 To determine whether the loss of non-neutralizing antibodies over time was due to preferential  
185 loss of antibodies targeting specific epitopes, we performed BLI experiments in which a  
186 preformed antibody-RBD complex was exposed to a second monoclonal targeting one of 3  
187 classes of structurally defined epitopes<sup>3,23</sup> (see schematic in Fig. 4a). We assayed 60 randomly  
188 selected antibodies with comparable neutralizing activity from the 1.3- and 12-month time  
189 points. The 60 antibodies were evenly distributed between the 2 time points and between  
190 neutralizers and non-neutralizers (Fig. 4). Antibody affinities for RBD were similar among  
191 neutralizers and non-neutralizers obtained at the same time point (Fig. 4b, Extended Data Fig. 8).  
192 When the two sets of un-related antibodies obtained from 1.3 and 12 months were compared,  
193 they showed significantly increased affinity over time irrespective of their neutralizing activity  
194 (Fig. 4b, Extended Data Fig. 8). In competition experiments, all but 2 of the 30 non-neutralizing  
195 antibodies failed to inhibit binding of the class 1 (C105), 2 (C121 and C144) or 3 (C135)  
196 antibodies tested and therefore must bind to epitopes that do not overlap with the epitopes of  
197 these classes of antibodies (Fig. 4c, and Extended Data Fig. 9). In contrast, all but 2 of the 30  
198 neutralizers blocked class 1, or 2 antibodies whose target epitopes are structural components of  
199 the RBD that interact with its cellular receptor, the angiotensin-converting enzyme 2<sup>23,24</sup> (ACE2)  
200 (Fig. 4c and Extended Data Fig. 9). In addition, whereas 9 of the 15 neutralizing antibodies  
201 obtained after 1.3 months blocked both class 1 and 2 antibodies, only 1 of the 15 obtained after  
202 12 months did so. In contrast to the earlier time point, 13 of 15 neutralizing antibodies obtained  
203 after 12 months only interfered with C121, a class 2 antibody<sup>3,23</sup> (Fig. 4c and Extended Data Fig.  
204 9). We conclude that neutralizing antibodies are retained and non-neutralizing antibodies  
205 targeting RBD surfaces that do not interact with ACE2 are removed from the repertoire over  
206 time.

207

208 To determine whether there was an increase in neutralization breadth over time, the neutralizing  
209 activity of the 60 antibodies was assayed against a panel of RBD mutants covering residues  
210 associated with circulating variants of concern: R346S, K417N, N440K, A475V, E484K and  
211 N501Y (Fig. 4d and Supplementary Table 6). Increased activity was evident against K417N,  
212 N440K, A475V, E484K and N501Y (Fig. 4d and Supplementary Table 6). We conclude that  
213 evolution of the antibody repertoire results in acquisition of neutralization breadth over time.

214

215 The increase in breadth and overall potency of memory B cell antibodies could be due to shifts in  
216 the repertoire, clonal evolution, or both. To determine whether changes in specific clones are  
217 associated with increases in affinity and breadth, we measured the relative affinity and  
218 neutralizing breadth of matched pairs of antibodies expressed by expanded clones of B cells that  
219 were maintained in the repertoire over the entire observation period<sup>3,4</sup>. SARS-CoV-2 neutralizing  
220 activity of the antibodies present at 1.3 or 12 months was not significantly correlated with  
221 affinity at either time point when each time point is considered independently (Fig. 4e).

222 However, there was a significant increase in overall affinity over time including in the 4 pairs of  
223 antibodies with no measurable neutralizing activity (Fig. 4f and Supplementary Table 7).

224 Neutralizing breadth was assayed for 15 randomly selected pairs of antibodies targeting epitopes  
225 assigned to the 3 dominant classes of neutralizing antibodies<sup>3,23,25,26</sup>. Seven of the selected  
226 antibodies showed equivalent or decreased activity against wild-type SARS-CoV-2 after 12  
227 months (Fig. 4g and Supplementary Table 8). However, neutralizing breadth increased between  
228 1.3 and 12-months for all 15 pairs, even when neutralizing activity against the wild-type was  
229 unchanged or decreased (Fig. 4g and Supplementary Table 8). Only 1 of the 15 antibodies

230 obtained after 1.3 months neutralized all the mutants tested (Fig. 4g). In contrast, 10 of the 15  
231 antibodies obtained from the same clones after 12 months neutralized all variants tested with  
232  $IC_{50}$ s as low as 1 ng/ml against the triple mutant K417N/E484K/N501Y found in B.1.351 (Fig.  
233 4g and Supplementary Table 8). Similar results were obtained with authentic WA1/2020 and  
234 B.1.351 (Extended Data Fig 7i). In conclusion, continued clonal evolution of anti-SARS-CoV-2  
235 antibodies over 12 months favors increasing potency and breadth resulting in monoclonal  
236 antibodies with exceptional activity against a broad group of variants.

237

## 238 **Discussion**

239 During immune responses activated B cells interact with cognate T cells and begin dividing  
240 before selection into the plasma cell, memory or germinal center B cell compartments based in  
241 part on their affinity for antigen<sup>17,27-31</sup>. Whereas B cells expressing high affinity antibodies are  
242 favored to enter the long-lived plasma cell compartment, the memory compartment is more  
243 diverse and can develop directly from activated B cells or from a germinal center<sup>17,27-31</sup>.  
244 Memory cells emanating from a germinal center carry more mutations than those that develop  
245 directly from activated B cells because they undergo additional cycles of division<sup>32</sup>.

246

247 Consistent with the longevity of bone marrow plasma cells, infection with SARS-CoV-2 leads to  
248 persistent serum anti-RBD antibodies, and corresponding neutralizing responses. Nearly 93% of  
249 the plasma neutralizing activity is retained between 6- and 12-months<sup>33,34</sup>. Vaccination boosts the  
250 neutralizing response by 1.5 orders of magnitude by inducing additional plasma cell  
251 differentiation from the memory B cell compartment<sup>5,7,35</sup>. Recruitment of evolved memory B  
252 cells producing antibodies with broad and potent neutralizing activity into the plasma cell

253 compartment is likely to account for the exceptional serologic activity of vaccinated  
254 convalescents against variants of concern<sup>20,35,36</sup>.

255

256 Less is known about selection and maintenance of the memory B cell compartment. SARS-CoV-  
257 2 infection produces a memory compartment that continues to evolve over 12 months after  
258 infection with accumulation of somatic mutations, emergence of new clones, and increasing  
259 affinity all of which is consistent with long-term persistence of germinal centers. The increase in  
260 activity against SARS-CoV-2 mutants parallels the increase in affinity and is consistent with the  
261 finding that increasing the apparent affinity of anti-SARS-CoV-2 antibodies by dimerization or  
262 by creating bi-specific antibodies also increases resistance to RBD mutations<sup>37-40</sup>.

263

264 Continued antibody evolution in germinal centers requires antigen which can be retained in these  
265 structures over long periods of time<sup>29</sup>. In addition, SARS-CoV-2 protein and nucleic acid has  
266 been reported in the gut for at least 2 months after infection<sup>4</sup>. Irrespective of the source of  
267 antigen, antibody evolution favors epitopes overlapping with the ACE2 binding site on the RBD,  
268 possibly because these are epitopes that are preferentially exposed on trimeric spike protein or  
269 virus particles.

270

271 Vaccination after SARS-CoV-2 infection increases the number of RBD binding memory cells by  
272 over an order of magnitude by recruiting new B cell clones into memory and expanding  
273 persistent clones. The persistent clones expand without accumulating large numbers of additional  
274 mutations indicating that clonal expansion of human memory B cells does not require re-entry  
275 into germinal centers and occurs through the activated B cell compartment<sup>17,27-31</sup>.

276

277 The remarkable evolution of breadth after infection and the robust enhancement of serologic  
 278 responses and B cell memory achieved with mRNA vaccination suggests that convalescent  
 279 individuals who are vaccinated should enjoy high levels of protection against emerging variants  
 280 without a need to modify existing vaccines. If memory responses evolve in a similar manner in  
 281 naive individuals that receive vaccines, additional appropriately timed boosting with available  
 282 vaccines should lead to protective immunity against circulating variants.

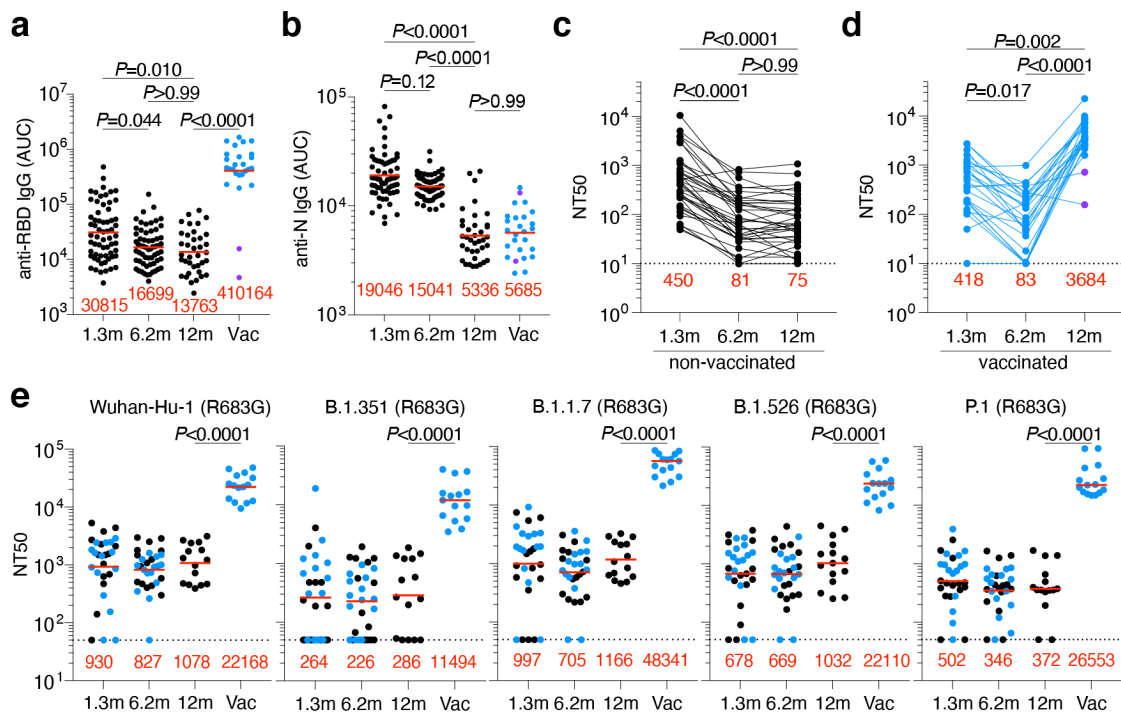
283

284

285

286

287 **Figures**

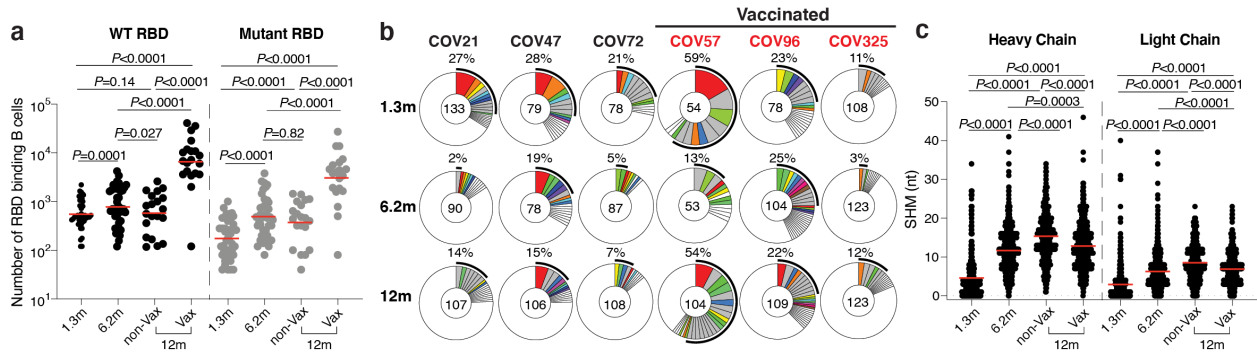


288

289 **Fig. 1: Plasma ELISAs and neutralizing activity. a-b**, Plasma IgG antibody binding to SARS-  
290 CoV-2 RBD (**a**) and N protein (**b**), and plasma neutralizing activity (**c-d**) 12 months after infection  
291 (n=63). **a** and **b**, Area under the curve (AUC) over time in non-vaccinated and vaccinated  
292 individuals, as indicated. Numbers in red indicate geometric mean AUC at the indicated timepoint.  
293 n=63, 37 convalescent and 26 convalescent vaccinated individuals. Statistical significance in **a** and  
294 **b** was determined using two-sided Kruskal-Wallis test with subsequent Dunn's multiple  
295 comparisons. **c, d**, NT50 over time in non-vaccinated (**c**) and vaccinated individuals (**d**). Lines  
296 connect longitudinal samples from the same individual. Statistical significance in **c-d** was  
297 determined using two-sided Friedman test with subsequent Dunn's multiple comparisons. Two  
298 individuals who received their first dose of vaccine 24-48 hours before sample collection are  
299 depicted in purple. **e**, Plasma neutralizing activity against indicated SARS-CoV-2 variants of  
300 concern (n=30, 15 convalescent and 15 convalescent vaccinated individuals). The B.1.526 variant  
301 used here does contain the E484K substitution. Please refer to Methods for a detailed list of all  
302 substitutions/deletions/insertions of spike variants used here. Convalescent and convalescent  
303 vaccinated individuals in **a-e** are shown in black and blue, respectively. Statistical significance was  
304 determined using two-tailed Mann-Whitney test. Red numbers in c-e indicate the geometric mean  
305 NT50 at the indicated timepoint. All experiments were performed at least in duplicate.

306

307



308

309 **Fig. 2: Anti-SARS-CoV-2 RBD B cell memory.** **a**, graph summarizes number of antigen binding

310 memory B cells per 2 million B cells (Extended data Fig 5b and c) obtained at 1.3, 6.2 and 12

311 months from 40 randomly selected individuals (vaccinees  $n=20$ , and non-vaccinees,  $n=20$ ). Each

312 dot is one individual. Red horizontal bars indicate geometric mean values. Statistical significance

313 was determined using two-sided Kruskal-Wallis test with subsequent Dunn's multiple

314 comparisons. **b**, Pie charts show the distribution of antibody sequences from 6 individuals after

315 1.3<sup>3</sup> (upper panel) or 6.2<sup>4</sup> (middle panel) or 12 months (lower panel). The number in the inner

316 circle indicates the number of sequences analyzed for the individual denoted above the circle. Pie

317 slice size is proportional to the number of clonally related sequences. The black outline indicates

318 the frequency of clonally expanded sequences detected in each participant. Colored slices indicate

319 persisting clones (same IGV and IGJ genes, with highly similar CDR3s) found at both timepoints

320 in the same participant. Grey slices indicate clones unique to the timepoint. White indicates

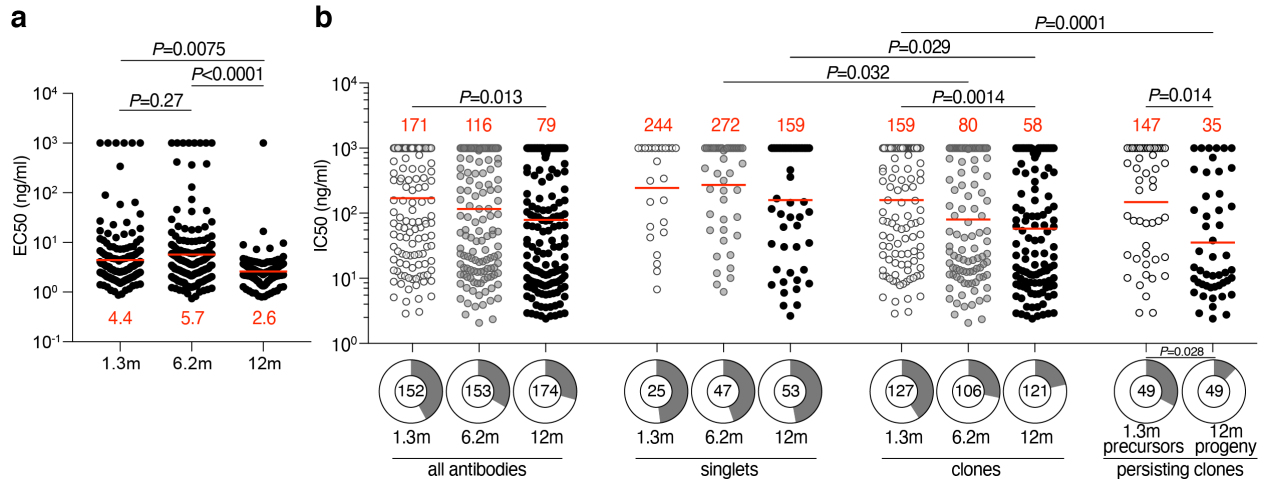
321 sequences isolated once, and white slices indicate singlets found at both timepoints. **c**. Number of

322 somatic nucleotide mutations in the IGVH and IGVL in antibodies (also Supplementary table 3)

323 obtained after 1.3 or 6.2 or 12 months (1.3m:  $n=889$ ; 6.2m:  $n=975$ ; 12m:  $n=1105$ , (non-vax:  $n=417$ ;

324 vax:  $n=688$ )). Red horizontal bars indicate mean values. Statistical significance was determined

325 using two-sided Kruskal-Wallis test with subsequent Dunn's multiple comparisons.



326

327 **Fig. 3: Anti-SARS-CoV-2 RBD monoclonal antibodies.** **a**, Graph shows the ELISA binding

328 EC<sub>50</sub> (Y axis) for SARS-CoV-2 RBD by antibodies isolated at 1.3<sup>3</sup> (n=152) 6.2<sup>4</sup> (n=153) and 12

329 months (n=174) after infection. Statistical significance was determined using the two-sided

330 Kruskal-Wallis test with subsequent Dunn's multiple comparisons (1.3 vs 6.2 months, p=0.27; 1.3

331 vs 12 months, p=0.0075; 6.2 vs 12 months, p<0.0001). **b**, Graph shows anti-SARS-CoV-2

332 neutralizing activity of monoclonal antibodies measured by a SARS-CoV-2 pseudovirus

333 neutralization assay<sup>3,13</sup>. Half-maximal inhibitory concentration (IC<sub>50</sub>) values for antibodies

334 isolated at 1.3<sup>3</sup> 6.2<sup>4</sup> and 12 months after infection against wild-type SARS-CoV-2 (Wuhan-Hu-1

335 strain<sup>41</sup>) are shown. Each dot represents one antibody. Pie charts illustrate the fraction of non-

336 neutralizing (IC<sub>50</sub> > 1000 ng/ml) antibodies (grey slices), inner circle shows the number of

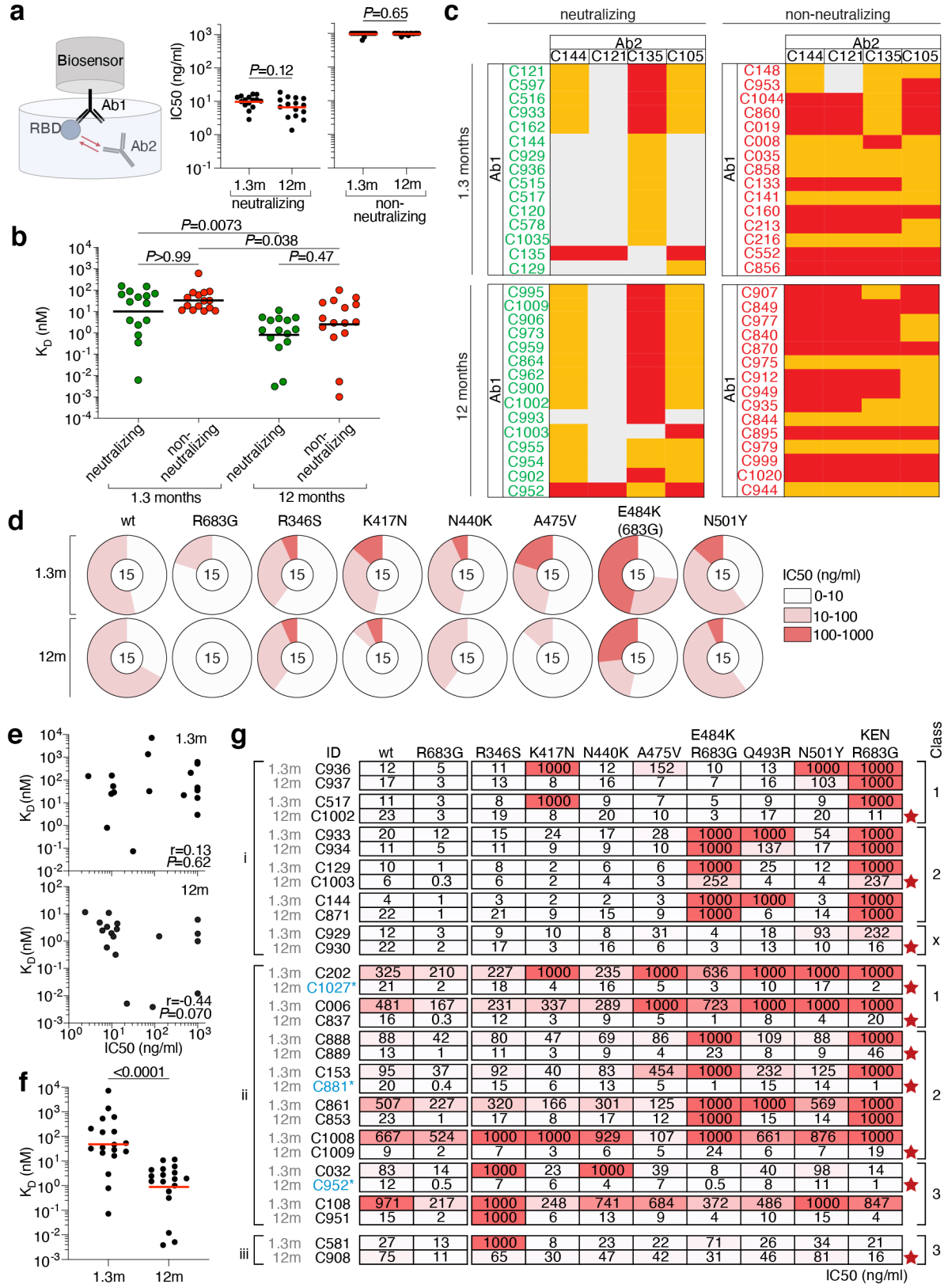
337 antibodies tested per group. Horizontal bars and red numbers indicate geometric mean values.

338 Statistical significance was determined through the two-sided Kruskal Wallis test with subsequent

339 Dunn's multiple comparisons.

340





342 **Fig. 4: Epitope targeting and evolution of anti-SARS-CoV-2 RBD antibodies.** **a**, Schematic  
343 representation of the BLI experiment (left) and  $IC_{50}$  values for randomly selected neutralizing  
344 (middle) and non-neutralizing (right) antibodies isolated at 1.3- and 12-months post-infection  
345 (each presented group shows  $n=15$  antibodies, resulting in a total of  $n=60$  antibodies). Red  
346 horizontal bars indicate geometric mean. Statistical significance was determined using two-sided  
347 Mann-Whitney test. **b**,  $K_D$  values of the  $n=30$  neutralizing (green) and  $n=30$  non-neutralizing (red)  
348 antibodies shown in **a**. Horizontal bars indicate geometric mean values. Statistical significance was  
349 determined using two-sided Kruskal Wallis test with subsequent Dunn's multiple comparisons.  
350 BLI traces can be found in Extended data Fig. 8. **c**, Heat-map of relative inhibition of Ab2 binding  
351 to the preformed Ab1-RBD complexes (grey=no binding, orange=intermediate binding, red=high  
352 binding). Values are normalized through the subtraction of the autologous antibody control. BLI  
353 traces can be found in Extended Data Fig 9. **d**, Neutralization of the indicated mutants for  
354 antibodies shown in panel **a-c**. Pie charts illustrate the fraction of antibodies that are poorly/non-  
355 neutralizing ( $IC_{50}$  100-1000 ng/ml, red), intermediate neutralizing ( $IC_{50}$  10-100 ng/ml, pink) and  
356 potentially neutralizing ( $IC_{50}$  0-10 ng/ml, white) for each mutant. Number in inner circle shows  
357 number of antibodies tested. **e**, Graphs show affinities (Y axis) plotted against neutralization  
358 activity (X axis) for 18 clonal antibody pairs isolated 1.3 (top) and 12 months (bottom) (after  
359 infection ( $n=36$  antibodies)). Statistical significance was determined using Spearman correlation  
360 test. **f**, BLI affinity measurements for same  $n=36$  paired 1.3- and 12-month antibodies as in **e**.  
361 Statistical significance was determined using two-tailed Wilcoxon test. **g**,  $IC_{50}$  values for  $n=30$   
362 paired neutralizing antibodies isolated at indicated timepoints against indicated mutant SARS-  
363 CoV-2 pseudoviruses. Antibodies are divided into groups i-iii, based on neutralizing activity: (i)  
364 potent clonal pairs that do not improve over time, (ii) clonal pairs that show increased activity over

365 time, and (iii) and clonal pairs showing decreased neutralization activity after 12 months. Antibody  
366 class assignment based on initial (1.3m) sensitivity to mutation is indicated on the right. Red stars  
367 indicate antibodies that neutralize all RBD mutants tested. Color gradient indicates IC<sub>50</sub> values  
368 ranging from 0 (white) to 1000 ng/ml (red).

369

370

371 **Methods**

372 **Study participants.**

373 Previously enrolled study participants were asked to return for a 12-month follow-up visit at the  
374 Rockefeller University Hospital in New York from February 8 to March 26, 2021. Eligible  
375 participants were adults with a history of participation in both prior study visits of our longitudinal  
376 cohort study of COVID-19 recovered individuals<sup>3,4</sup>. All participants had a confirmed history of  
377 SARS-CoV-2 infection, either diagnosed during the acute infection by RT-PCR or retrospectively  
378 confirmed by seroconversion. Exclusion criteria included presence of symptoms suggestive of  
379 active SARS-CoV-2 infection. Most study participants were residents of the Greater New York  
380 City tri-state region and were asked to return approximately 12 months after the time of onset of  
381 COVID-19 symptoms. Participants presented to the Rockefeller University Hospital for blood  
382 sample collection and were asked about potential symptom persistence since their 6.2-month study  
383 visit, laboratory-confirmed episodes of reinfection with SARS-CoV-2, and whether they had  
384 received any COVID-19 related treatment or SARS-CoV-2 vaccination in the interim. Study  
385 participants who had received COVID-19 vaccinations, were exclusively recipients of one of the  
386 two currently EUA-approved mRNA vaccines, Moderna (mRNA-1273) or Pfizer-BioNTech  
387 (BNT162b2), and individuals who received both doses did so according to current interval  
388 guidelines, namely 28 days (range 28-30 days) for Moderna and 21 days (range 21-23 days) for  
389 Pfizer-BioNtech. Detailed characteristics of the symptomology and severity of the acute infection,  
390 symptom kinetics, and the immediate convalescent phase (7 weeks post-symptom onset until  
391 6.2month visit) have been reported previously <sup>4</sup>. Participants that presented with persistent  
392 symptoms attributable to COVID-19 were identified on the basis of chronic shortness of breath or  
393 fatigue, deficit in athletic ability and/or three or more additional long-term symptoms such as

394 persistent unexplained fevers, chest pain, new-onset cardiac sequelae, arthralgias, impairment of  
395 concentration/mental acuity, impairment of sense of smell/taste, neuropathy or cutaneous findings  
396 as previously described <sup>4</sup>. Clinical data collection and management were carried out using the  
397 software iRIS by iMedRIS. All participants at Rockefeller University provided written informed  
398 consent before participation in the study and the study was conducted in accordance with Good  
399 Clinical Practice. For detailed participant characteristics see Supplementary Table 2. The study  
400 was performed in compliance with all relevant ethical regulations and the protocol (DRO-1006)  
401 for studies with human participants was approved by the Institutional Review Board of the  
402 Rockefeller University.

403

#### 404 **SARS-CoV-2 molecular tests**

405 Saliva was collected into guanidine thiocyanate buffer as described <sup>42</sup>. RNA was extracted using  
406 either a column-based (Qiagen QIAmp DSP Viral RNA Mini Kit, Cat#61904) or a magnetic bead-  
407 based method as described <sup>43</sup>. Reverse transcribed cDNA was amplified using primers and probes  
408 validated by the CDC or by Columbia University Personalized Medicine Genomics Laboratory  
409 respectively and approved by the FDA under the Emergency Use Authorization. Viral RNA was  
410 considered detected if Ct for two viral primers/probes were <40.

411

#### 412 **Blood samples processing and storage.**

413 Peripheral Blood Mononuclear Cells (PBMCs) obtained from samples collected at Rockefeller  
414 University were purified as previously reported by gradient centrifugation and stored in liquid  
415 nitrogen in the presence of FCS and DMSO <sup>3,4</sup>. Heparinized plasma and serum samples were

416 aliquoted and stored at -20 °C or less. Prior to experiments, aliquots of plasma samples were  
417 heat-inactivated (56 °C for 1 hour) and then stored at 4 °C.

418

#### 419 **ELISAs**

420 ELISAs<sup>44,45</sup> to evaluate antibodies binding to SARS-CoV-2 RBD and N were performed by  
421 coating of high-binding 96-half-well plates (Corning 3690) with 50 µl per well of a 1µg/ml  
422 protein solution in PBS overnight at 4 °C. Plates were washed 6 times with washing buffer (1×  
423 PBS with 0.05% Tween-20 (Sigma-Aldrich)) and incubated with 170 µl per well blocking buffer  
424 (1× PBS with 2% BSA and 0.05% Tween-20 (Sigma)) for 1 h at room temperature. Immediately  
425 after blocking, monoclonal antibodies or plasma samples were added in PBS and incubated for 1  
426 h at room temperature. Plasma samples were assayed at a 1:66 starting dilution and 7 (IgA and  
427 IgM anti-RBD) or 11 (IgG anti-RBD) additional threefold serial dilutions. Monoclonal  
428 antibodies were tested at 10 µg/ml starting concentration and 10 additional fourfold serial  
429 dilutions. Plates were washed 6 times with washing buffer and then incubated with anti-human  
430 IgG, IgM or IgA secondary antibody conjugated to horseradish peroxidase (HRP) (Jackson  
431 Immuno Research 109-036-088 109-035-129 and Sigma A0295) in blocking buffer at a 1:5,000  
432 dilution (IgM and IgG) or 1:3,000 dilution (IgA). Plates were developed by addition of the HRP  
433 substrate, TMB (ThermoFisher) for 10 min (plasma samples) or 4 minutes (monoclonal  
434 antibodies). The developing reaction was stopped by adding 50 µl 1 M H<sub>2</sub>SO<sub>4</sub> and absorbance  
435 was measured at 450 nm with an ELISA microplate reader (FluoStar Omega 5.11, BMG  
436 Labtech) with Omega MARS software for analysis. For plasma samples, a positive control  
437 (plasma from participant COV72, diluted 66.6-fold and seven additional threefold serial dilutions  
438 in PBS) was added to every assay plate for validation. The average of its signal was used for

439 normalization of all of the other values on the same plate with Excel software before calculating  
440 the area under the curve using Prism V9.1(GraphPad). For monoclonal antibodies, the EC50 was  
441 determined using four-parameter nonlinear regression (GraphPad Prism V9.1).

442

#### 443 **Proteins**

444 Mammalian expression vectors encoding the RBDs of SARS-CoV-2 (GenBank MN985325.1; S  
445 protein residues 319-539) or K417N, E484K, N501Y RBD mutants with an N-terminal human  
446 IL-2 or Mu phosphatase signal peptide were previously described <sup>46</sup>. SARS-CoV-2 nucleocapsid  
447 protein (N) was purchased from Sino Biological (40588-V08B).

448

#### 449 **SARS-CoV-2 pseudotyped reporter virus**

450 A panel of plasmids expressing RBD-mutant SARS-CoV-2 spike proteins in the context of  
451 pSARS-CoV-2-S<sub>Δ19</sub> has been described previously <sup>2,9,26</sup>. Variant pseudoviruses resembling  
452 variants of concern B.1.1.7 (first isolated in the UK), B.1.351 (first isolated in South-Africa),  
453 B.1.526 (first isolated in New York City) and P.1 (first isolated in Brazil) were generated by  
454 introduction of substitutions using synthetic gene fragments (IDT) or overlap extension PCR  
455 mediated mutagenesis and Gibson assembly. Specifically, the variant-specific deletions and  
456 substitutions introduced were:

457 B.1.1.7: ΔH69/V70, ΔY144, N501Y, A470D, D614G, P681H, T761I, S982A, D118H

458 B.1.351: D80A, D215G, L242H, R246I, K417N, E484K, N501Y, D614G, A701V

459 B.1.526: L5F, T95I, D253G, E484K, D614G, A701V.

460 P.1: L18F, R20N, P26S, D138Y, R190S, K417T, E484K, N501Y, D614G, H655Y

461

462

463 The E484K and K417N/E484K/N501Y (KEN) substitution, as well as the deletions/substitutions  
464 corresponding to variants of concern were incorporated into a spike protein that also includes the  
465 R683G substitution, which disrupts the furin cleavage site and increases particle infectivity.  
466 Neutralizing activity against mutant pseudoviruses were compared to a wildtype SARS-CoV-2  
467 spike sequence (NC\_045512), carrying R683G where appropriate.

468 SARS-CoV-2 pseudotyped particles were generated as previously described<sup>3,13</sup>. Briefly, 293T  
469 cells were transfected with pNL4-3ΔEnv-nanoluc and pSARS-CoV-2-S<sub>Δ19</sub>, particles were  
470 harvested 48 hpt, filtered and stored at -80°C.

471

#### 472 **Microneutralization assay with authentic SARS-CoV-2.**

473 Microneutralization assay of SARS-CoV-2 virus were performed as described previously<sup>3</sup>. The  
474 day prior to infection, Vero E6 cells were seeded at  $1 \times 10^4$  cells/well into 96-well plates. The  
475 diluted plasma and antibodies were mixed with SARS-CoV-2 WA1/2020 or the SA variant  
476 B.1.351 and incubated for 1 hour at 37°C. The antibody-virus-mix was then directly applied to  
477 Vero E6 cells and incubated for 22 hours at 37°C. Cells were subsequently fixed by adding an  
478 equal volume of 70% formaldehyde to the wells, followed by permeabilization with 1% Triton  
479 X-100 for 10 minutes. After washing, cells were incubated for 1 hour at 37°C with blocking  
480 solution of 5% goat serum in PBS (catalog no. 005-000-121; Jackson ImmunoResearch). A  
481 rabbit polyclonal anti-SARS-CoV-2 nucleocapsid antibody (catalog no. GTX135357; GeneTex)  
482 was added to the cells at 1:1,000 dilution in blocking solution and incubated at 4 °C overnight.  
483 Goat anti-rabbit AlexaFluor 594 (catalog no. A-11012; Life Technologies) was used as a  
484 secondary antibody at a dilution of 1:2000. Nuclei were stained with Hoechst 33342 (catalog no.



485 62249; Thermo Fisher Scientific) at 1 µg/ml. Images were acquired with a fluorescence  
486 microscope and analyzed using ImageXpress Micro XLS (Molecular Devices). All experiments  
487 were performed in a biosafety level 3 laboratory.

488

#### 489 **Pseudotyped virus neutralization assay**

490 Fourfold serially diluted plasma from COVID-19-convalescent individuals or monoclonal  
491 antibodies were incubated with SARS-CoV-2 pseudotyped virus for 1 h at 37 °C. The mixture  
492 was subsequently incubated with 293T<sub>Ace2</sub> cells<sup>3</sup> (for comparisons of plasma or monoclonal  
493 antibodies from convalescent individuals) or HT1080Ace2 cl14 cells<sup>13</sup> (for analyses involving  
494 mutant/variant pseudovirus panels), as indicated, for 48h after which cells were washed with  
495 PBS and lysed with Luciferase Cell Culture Lysis 5× reagent (Promega). Nanoluc Luciferase  
496 activity in lysates was measured using the Nano-Glo Luciferase Assay System (Promega) with  
497 the Glomax Navigator (Promega). The obtained relative luminescence units were normalized to  
498 those derived from cells infected with SARS-CoV-2 pseudotyped virus in the absence of plasma  
499 or monoclonal antibodies. The half-maximal neutralization titers for plasma (NT<sub>50</sub>) or half-  
500 maximal and 90% inhibitory concentrations for monoclonal antibodies (IC<sub>50</sub> and IC<sub>90</sub>) were  
501 determined using four-parameter nonlinear regression (least squares regression method without  
502 weighting; constraints: top=1, bottom=0) (GraphPad Prism).

503

#### 504 **Biotinylation of viral protein for use in flow cytometry**

505 Purified and Avi-tagged SARS-CoV-2 RBD or SARS-CoV-2 RBD KEN mutant (K417N,  
506 E484K, N501Y) was biotinylated using the Biotin-Protein Ligase-BIRA kit according to  
507 manufacturer's instructions (Avidity) as described before<sup>3</sup>. Ovalbumin (Sigma, A5503-1G) was

508 biotinylated using the EZ-Link Sulfo-NHS-LC-Biotinylation kit according to the manufacturer's  
509 instructions (Thermo Scientific). Biotinylated ovalbumin was conjugated to streptavidin-BV711  
510 (BD biosciences, 563262) and RBD to streptavidin-PE (BD Biosciences, 554061) and  
511 streptavidin-AF647 (Biolegend, 405237) <sup>3</sup>.

512

### 513 **Flow cytometry and single cell sorting**

514 Single-cell sorting by flow cytometry was described previously <sup>3</sup>. Briefly, peripheral blood  
515 mononuclear cells were enriched for B cells by negative selection using a pan-B-cell isolation kit  
516 according to the manufacturer's instructions (Miltenyi Biotec, 130-101-638). The enriched B  
517 cells were incubated in FACS buffer (1× PBS, 2% FCS, 1 mM EDTA) with the following anti-  
518 human antibodies (all at 1:200 dilution): anti-CD20-PECy7 (BD Biosciences, 335793), anti-  
519 CD3-APC-eFluoro 780 (Invitrogen, 47-0037-41), anti-CD8-APC-eFluoro 780 (Invitrogen, 47-  
520 0086-42), anti-CD16-APC-eFluoro 780 (Invitrogen, 47-0168-41), anti-CD14-APC-eFluoro 780  
521 (Invitrogen, 47-0149-42), as well as Zombie NIR (BioLegend, 423105) and fluorophore-labelled  
522 RBD and ovalbumin (Ova) for 30 min on ice. Single CD3-CD8-CD14-CD16-CD20+Ova-RBD-  
523 PE+RBD-AF647+ B cells were sorted into individual wells of 96-well plates containing 4 µl of  
524 lysis buffer (0.5× PBS, 10 mM DTT, 3,000 units/ml RNasin Ribonuclease Inhibitors (Promega,  
525 N2615) per well using a FACS Aria III and FACSDiva software (Becton Dickinson) for  
526 acquisition and FlowJo for analysis. The sorted cells were frozen on dry ice, and then stored at  
527 -80 °C or immediately used for subsequent RNA reverse transcription. For B cell phenotype  
528 analysis, in addition to above antibodies, B cells were also stained with following anti-human  
529 antibodies: anti- IgG-PECF594 (BD biosciences, 562538), anti-IgM-AF700 (Biolegend,  
530 314538), anti-IgA-Viogreen (Miltenyi Biotec, 130-113-481).

531

532 **Antibody sequencing, cloning and expression**

533 Antibodies were identified and sequenced as described previously<sup>3</sup>. In brief, RNA from single  
534 cells was reverse-transcribed (SuperScript III Reverse Transcriptase, Invitrogen, 18080-044) and  
535 the cDNA stored at  $-20^{\circ}\text{C}$  or used for subsequent amplification of the variable IGH, IGL and  
536 IGK genes by nested PCR and Sanger sequencing. Sequence analysis was performed using  
537 MacVector. Amplicons from the first PCR reaction were used as templates for sequence- and  
538 ligation-independent cloning into antibody expression vectors. Recombinant monoclonal  
539 antibodies were produced and purified as previously described<sup>3</sup>.

540

541 **Biolayer interferometry**

542 Biolayer interferometry assays were performed as previously described<sup>3</sup>. Briefly, we used the  
543 Octet Red instrument (ForteBio) at  $30^{\circ}\text{C}$  with shaking at 1,000 r.p.m. Epitope-binding assays  
544 were performed with protein A biosensor (ForteBio 18-5010), following the manufacturer's  
545 protocol 'classical sandwich assay'. (1) Sensor check: sensors immersed 30 s in buffer alone  
546 (kinetics buffer 10x ForteBio 18-1105 diluted 1x in PBS1x). (2) Capture first antibody: sensors  
547 immersed 10 min with Ab1 at  $30\ \mu\text{g}/\text{ml}$ . (3) Baseline: sensors immersed 30 s in buffer alone. (4)  
548 Blocking: sensors immersed 5 min with IgG isotype control at  $50\ \mu\text{g}/\text{ml}$ . (6) Antigen association:  
549 sensors immersed 5 min with RBD at  $100\ \mu\text{g}/\text{ml}$ . (7) Baseline: sensors immersed 30 s in buffer  
550 alone. (8) Association Ab2: sensors immersed 5 min with Ab2 at  $30\ \mu\text{g}/\text{ml}$ . Curve fitting was  
551 performed using the Fortebio Octet Data analysis software (ForteBio). Affinity measurement of  
552 anti-SARS-CoV-2 IgGs binding were corrected by subtracting the signal obtained from traces  
553 performed with IgGs in the absence of WT RBD. The kinetic analysis using protein A biosensor

554 (ForteBio 18-5010) was performed as follows: (1) baseline: 60sec immersion in buffer. (2)  
555 loading: 200sec immersion in a solution with IgGs 30  $\mu\text{g/ml}$ . (3) baseline: 200sec immersion in  
556 buffer. (4) Association: 300sec immersion in solution with WT RBD at 200, 100, 50 or 25  $\mu\text{g/ml}$   
557 (5) dissociation: 600sec immersion in buffer. Curve fitting was performed using a fast 1:1  
558 binding model and the Data analysis software (ForteBio). Mean  $K_D$  values were determined by  
559 averaging all binding curves that matched the theoretical fit with an  $R^2$  value  $\geq 0.8$ .

560

### 561 **Plasma antibody avidity assay**

562 The plasma SARS-CoV-2 antibody avidity assay were performed as previously described <sup>47</sup>.

563

### 564 **Computational analyses of antibody sequences**

565 Antibody sequences were trimmed based on quality and annotated using Igbblastn v.1.14. with  
566 IMGT domain delineation system. Annotation was performed systematically using Change-O  
567 toolkit v.0.4.540 <sup>48</sup>. Heavy and light chains derived from the same cell were paired, and  
568 clonotypes were assigned based on their V and J genes using in-house R and Perl scripts (Fig.  
569 2d). All scripts and the data used to process antibody sequences are publicly available on GitHub  
570 (<https://github.com/stratust/igpipeline>).

571

572 The frequency distributions of human V genes in anti-SARS-CoV-2 antibodies from this study  
573 was compared to 131,284,220 IgH and IgL sequences generated by <sup>49</sup> and downloaded from  
574 cAb-Rep<sup>50</sup>, a database of human shared BCR clonotypes available at [https://cab-](https://cab-rep.c2b2.columbia.edu/)  
575 [rep.c2b2.columbia.edu/](https://cab-rep.c2b2.columbia.edu/). Based on the 91 distinct V genes that make up the 6902 analyzed  
576 sequences from Ig repertoire of the 10 participants present in this study, we selected the IgH and

577 IgL sequences from the database that are partially coded by the same V genes and counted them  
578 according to the constant region. The frequencies shown in (Extended data Fig. 4) are relative to  
579 the source and isotype analyzed. We used the two-sided binomial test to check whether the  
580 number of sequences belonging to a specific IgHV or IGLV gene in the repertoire is different  
581 according to the frequency of the same IgV gene in the database. Adjusted p-values were  
582 calculated using the false discovery rate (FDR) correction. Significant differences are denoted  
583 with stars.

584

585 Nucleotide somatic hypermutation and CDR3 length were determined using in-house R and Perl  
586 scripts. For somatic hypermutations, IGHV and IGLV nucleotide sequences were aligned against  
587 their closest germlines using Igblastn and the number of differences were considered nucleotide  
588 mutations. The average mutations for V genes were calculated by dividing the sum of all  
589 nucleotide mutations across all participants by the number of sequences used for the analysis.

590

591 Immunoglobulins grouped into the same clonal lineage had their respective IgH and IgL sequences  
592 merged and subsequently aligned, using TranslatorX v.1.1<sup>51</sup>, with the unmutated ancestral  
593 sequence obtained from IMGT/V-QUEST reference directory<sup>52</sup>. GCTree  
594 (<https://github.com/matsengrp/gctree>)<sup>53</sup> was further used to perform the phylogenetic trees  
595 construction. Each node represents a unique IgH and IgL combination and the size of each node is  
596 proportional to the number of identical sequences. The numbered nodes represent the unobserved  
597 ancestral genotypes between the germline sequence and the sequences on the downstream branch.

598 **Competing interests:** The Rockefeller University has filed a provisional patent application in  
599 connection with this work on which M.C.N. is an inventor (US patent 63/021,387). The patent

600 has been licensed by Rockefeller University to Bristol Meyers Squib. Z.Z. received seed  
601 instruments and sponsored research funding from ET Healthcare.

602

603 **Data availability statement:** Data are provided in SI Tables 1-8. The raw sequencing data and  
604 computer scripts associated with Figure 2 and Extended data figure 5 have been deposited at  
605 Github (<https://github.com/stratust/igpipeline>). This study also uses data from “A Public  
606 Database of Memory and Naive B-Cell Receptor Sequences”  
607 (<https://doi.org/10.5061/dryad.35ks2>) and from “High frequency of shared clonotypes in human  
608 B cell receptor repertoires” (<https://doi.org/10.1038/s41586-019-0934-8>).

609

610 **Code availability statement:** Computer code to process the antibody sequences is available at  
611 GitHub (<https://github.com/stratust/igpipeline>).

612

613

#### 614 **Data presentation**

615 Figures arranged in Adobe Illustrator 2020.

616

617 **Acknowledgements:** We thank all study participants who devoted time to our research; The  
618 Rockefeller University Hospital nursing staff and Clinical Research Support Office and nursing  
619 staff. Mayu Okawa Frank, Marissa Bergh, and Robert B. Darnell for SARS-CoV-2 saliva PCR  
620 testing. Pamela J. Bjorkman and all members of the M.C.N. laboratory for helpful discussions and  
621 Maša Jankovic for laboratory support. This work was supported by NIH grant P01-AI138398-S1  
622 (M.C.N., C.M.R and P.J.B.) and 2U19AI111825 (M.C.N. and C.M.R); George Mason University  
623 Fast Grants to C.M.R., 3 R01-AI091707-10S1 to C.M.R.; The G. Harold and Leila Y. Mathers

624 Charitable Foundation to C.M.R.; NIH grant R37-AI64003 to P.D.B.; NIH grant R01AI78788 to  
625 T.H.; We thank Dr. Jost Vielmetter and the Protein Expression Center in the Beckman Institute at  
626 Caltech for expression assistance. C.O.B. is supported by the HHMI Hanna Gray and Burroughs  
627 Wellcome PDEP fellowships. C.G. was supported by the Robert S. Wennett Post-Doctoral  
628 Fellowship, in part by the National Center for Advancing Translational Sciences (National  
629 Institutes of Health Clinical and Translational Science Award program, grant UL1 TR001866),  
630 and by the Shapiro-Silverberg Fund for the Advancement of Translational Research. P.D.B. and  
631 M.C.N. are Howard Hughes Medical Institute Investigators. F.M. is supported by the Bulgari  
632 Women & Science Fellowship in COVID-19 Research.

633

634 **Author Contributions:** P.D.B., T.H., C.M.R., and M.C.N. conceived, designed and analyzed the  
635 experiments. M. Caskey and C.G. designed clinical protocols. Z.W., F.M., D.S.B., S.F., C.V., H-  
636 H.H., C.O.B., A.C., F.S., J.D.S., E.B., L.A., J.Y., M.J. and Z.Z. carried out experiments. A.G. and  
637 M. Cipolla produced antibodies. D.S.B., M.D., M.T., K.G.M., C.G. and M. Caskey recruited  
638 participants, executed clinical protocols and processed samples. T.Y.O. and V.R. performed  
639 bioinformatic analysis. Z.W., F.M., D.S.B., C.G. and M.C.N. wrote the manuscript with input from  
640 all co-authors.

641

642

643

644

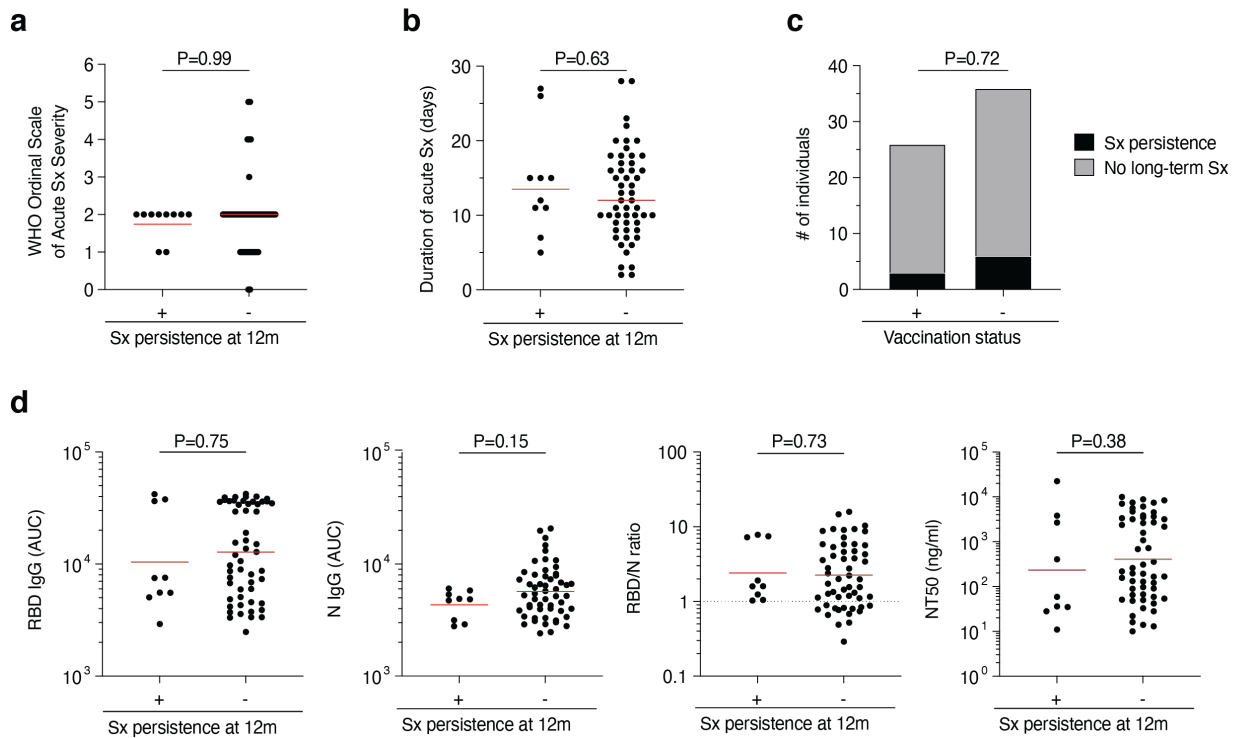
645

646

647

648

649 **Extended Data Figures**



650

651 **Extended Data Fig. 1 Clinical correlations. a-d**, Association of persistence of symptoms (Sx)

652 12 months after infection with various clinical and serological parameters in our cohort of

653 individuals who recovered from COVID-19 (n=63). **a-b**, Acute disease severity as assessed with

654 the WHO Ordinal Scale of Clinical Improvement (**a**, p=0.99) and duration of acute phase

655 symptoms (**b**, p=0.63) in individuals reporting persistent symptoms (+) compared to individuals

656 who are symptom-free (-) 12 months post-infection. **c**, Proportion of individuals reporting

657 persistent symptoms (black area) compared to individuals who are symptom-free (grey area) 12

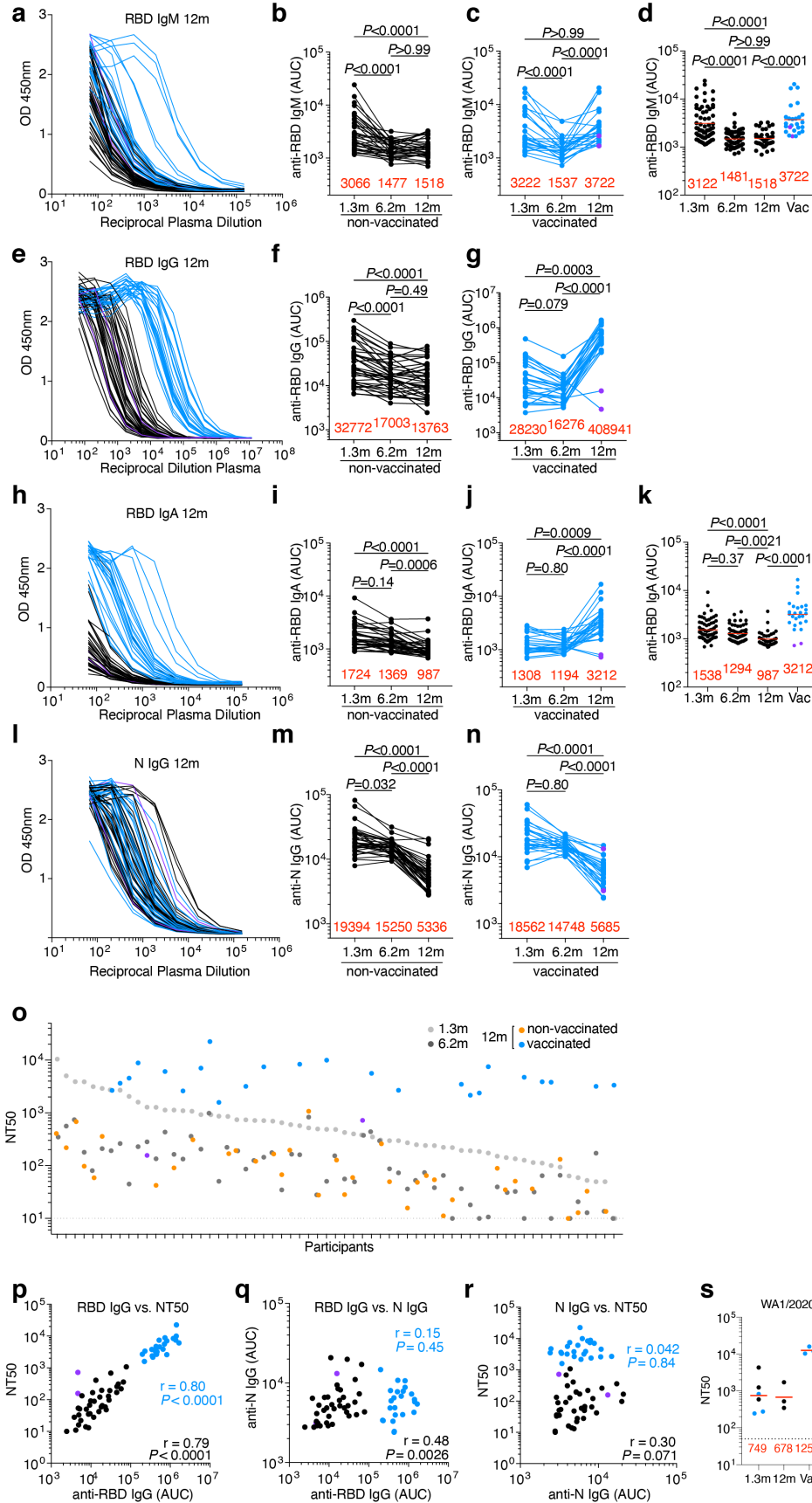
658 months after infection grouped by vaccination status (p=0.72). **d**, Anti-RBD IgG (p=0.75), anti-

659 N IgG (p=0.15), the RBD/N IgG ratio (p=0.73), and NT50 titers (p=0.38) at 12 months after

660 infection in individuals reporting persistent symptoms (+) compared to individuals who are



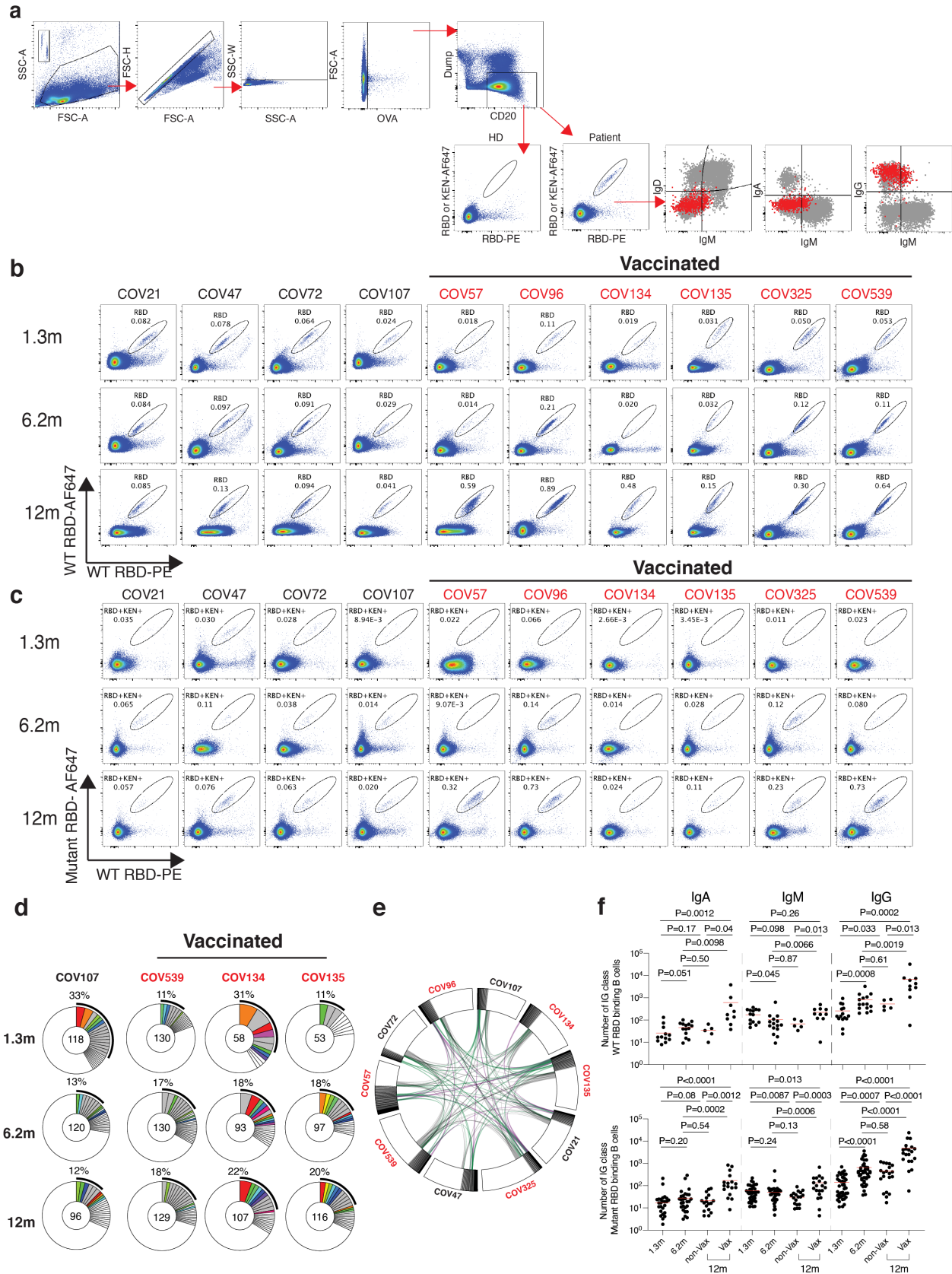
661 symptom-free (-) 12 months post-infection. Statistical significance was determined using the  
662 two-tailed Mann-Whitney test in **a**, **b** and **d**, and using the two-sided Fisher's exact test in **c**.



664 **Extended Data Fig. 2: Plasma activity. a-h**, ELISA results for plasma against SARS-CoV-2  
665 RBD 12 months after infection (n=63). Non-vaccinated individuals are depicted with black circles  
666 and lines, and vaccinated individuals are depicted in blue throughout. Two outlier individuals who  
667 received their first dose of vaccine 24-48 hours before sample collection is depicted as purple  
668 circles. **a-n**, IgM (**a-d**) IgG (**e-g**) and IgA (**h-k**) antibody binding to SARS-CoV-2 RBD and IgG  
669 binding to N (**l-n**) 12 months after infection. **a, e, h, l**, ELISA curves from non-vaccinated (black  
670 lines) individuals, as well as individuals who received one or two doses (blue lines) of a COVID-  
671 19 mRNA vaccine (left panels). Area under the curve (AUC) over time in non-vaccinated (**b, f, i**  
672 and **m**) and vaccinated individuals (**c, g, j, and n**). Lines connect longitudinal samples. **d, k**,  
673 Boxplots showing AUC values of all 63 individuals, as indicated. **o**, ranked average NT50 at 1.3  
674 months (light grey) and 6.2 months (dark grey), as well as at 12 months for non-vaccinated  
675 (orange) individuals, and individuals who received one or two doses (blue circles) of a COVID-  
676 19 mRNA vaccine, respectively. Two individuals who received their first dose of vaccine 24-48  
677 hours before sample collection is depicted in purple. **p-r**, Correlation of serological parameters in  
678 non-vaccinated (black circles and black statistics) and vaccinated (blue circles and blue statistics)  
679 individuals. Two individuals who received their first dose of vaccine 24-48 hours before sample  
680 collection is depicted as purple circles. Correlation of 12-month titers of anti- RBD IgG and NT50  
681 (**p**), anti-RBD IgG and N IgG (**q**), and anti-N IgG and NT50 (**r**). **s**, Plasma neutralizing activity  
682 against authentic virus isolates WA1/2020 and B.1.351, as indicated (n=6). Statistical significance  
683 was determined using two-sided Friedman test with subsequent Dunn's multiple comparisons  
684 (**b,c,f,g,i,j,m,n**), or two-sided Kruskal-Wallis test with subsequent Dunn's multiple comparisons  
685 (**d and k**) or using the Spearman correlation test for the non-vaccinated and vaccinated subgroups  
686 independently (**p-r**) or using two-tailed Mann-Whitney test (**s**). Red numbers indicate the

687 geometric mean NT50 at the indicated timepoint. All experiments were performed at least in  
688 duplicate.

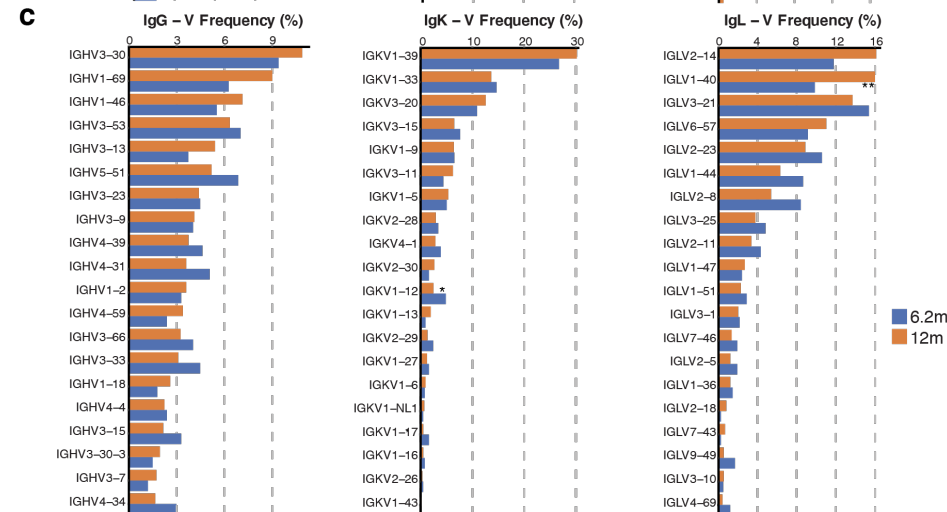
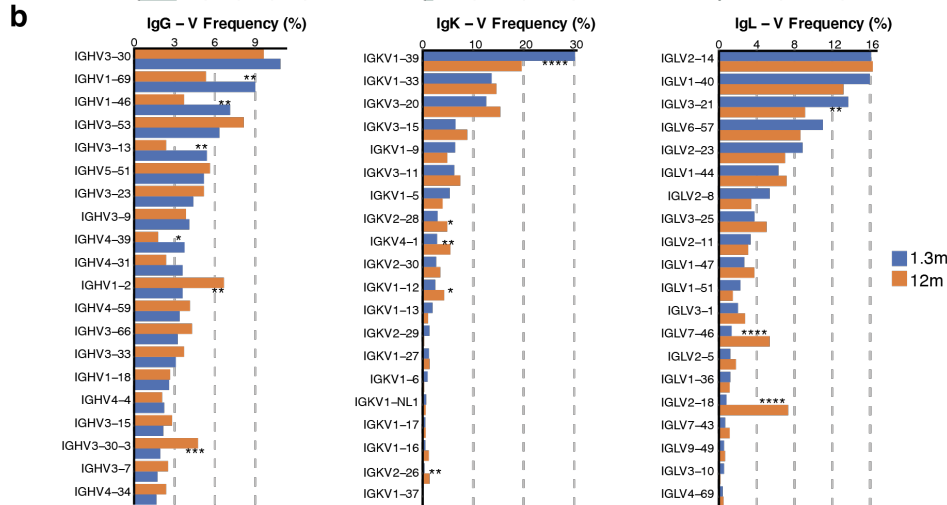
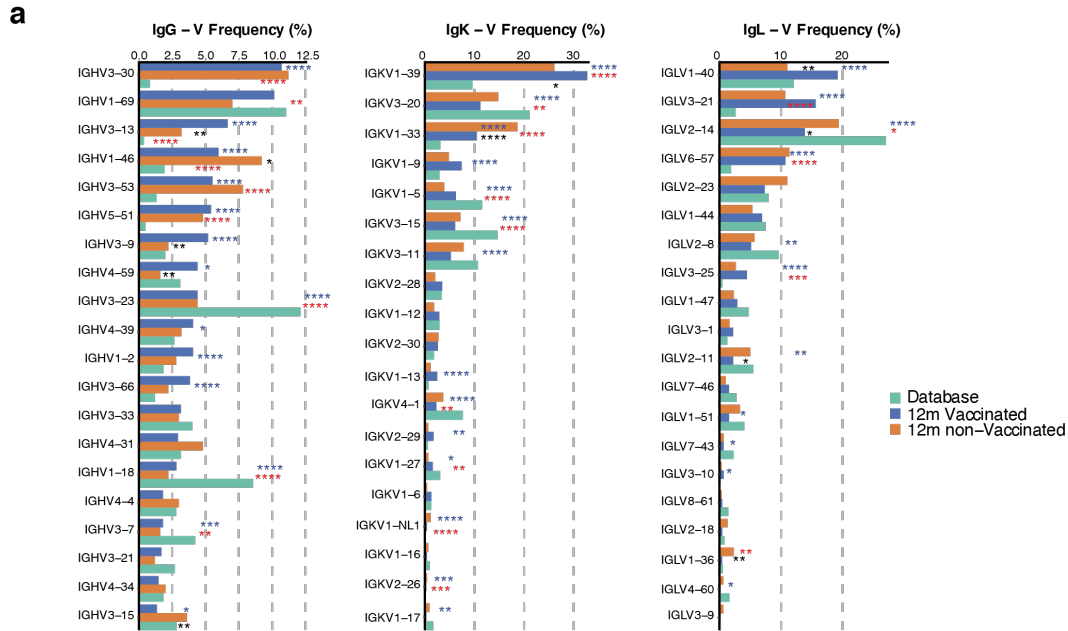
689



691 **Extended Data Fig. 3: Flow cytometry. a**, Gating strategy. Gating was on singlets that were  
692 CD20<sup>+</sup> and CD3-CD8-CD16-Ova-. Anti-IgG, IgM, and IgA antibodies were used for B cell  
693 phenotype analysis. Sorted cells were RBD-PE<sup>+</sup> and RBD/KEN-AF647<sup>+</sup>. **b and c**, Flow cytometry  
694 showing the percentage of RBD-double positive (**b**) and 647-K417N/E484K/N501Y mutant RBD  
695 cross-reactive (**c**) memory B cells from 1.3 or 6- and 12-months post-infection in 10 selected  
696 participants. **d**. as in Fig. 2b, Pie charts show the distribution of antibody sequences from 4  
697 individuals after 1.3<sup>3</sup> (upper panel) or 6.2<sup>4</sup> months (middle panel) or 12 months (lower panel). **e**,  
698 Circos plot depicts the relationship between antibodies that share V and J gene segment sequences  
699 at both IGH and IGL. Purple, green, and grey lines connect related clones, clones and singles, and  
700 singles to each other, respectively. **f**, graph summarizes cell number (indicated in **b** and **c**) (per 2  
701 million B cells) of immunoglobulin class of antigens binding memory B cells in samples obtained  
702 at 1.3, 6.2 and 12 months. Each dot is one individual. (Vaccinees, n=20, and non-vaccinees, n=20).  
703 Red horizontal bars indicate mean values. Statistical significance was determined using two-sided  
704 Kruskal-Wallis test with subsequent Dunn's multiple comparisons.

705

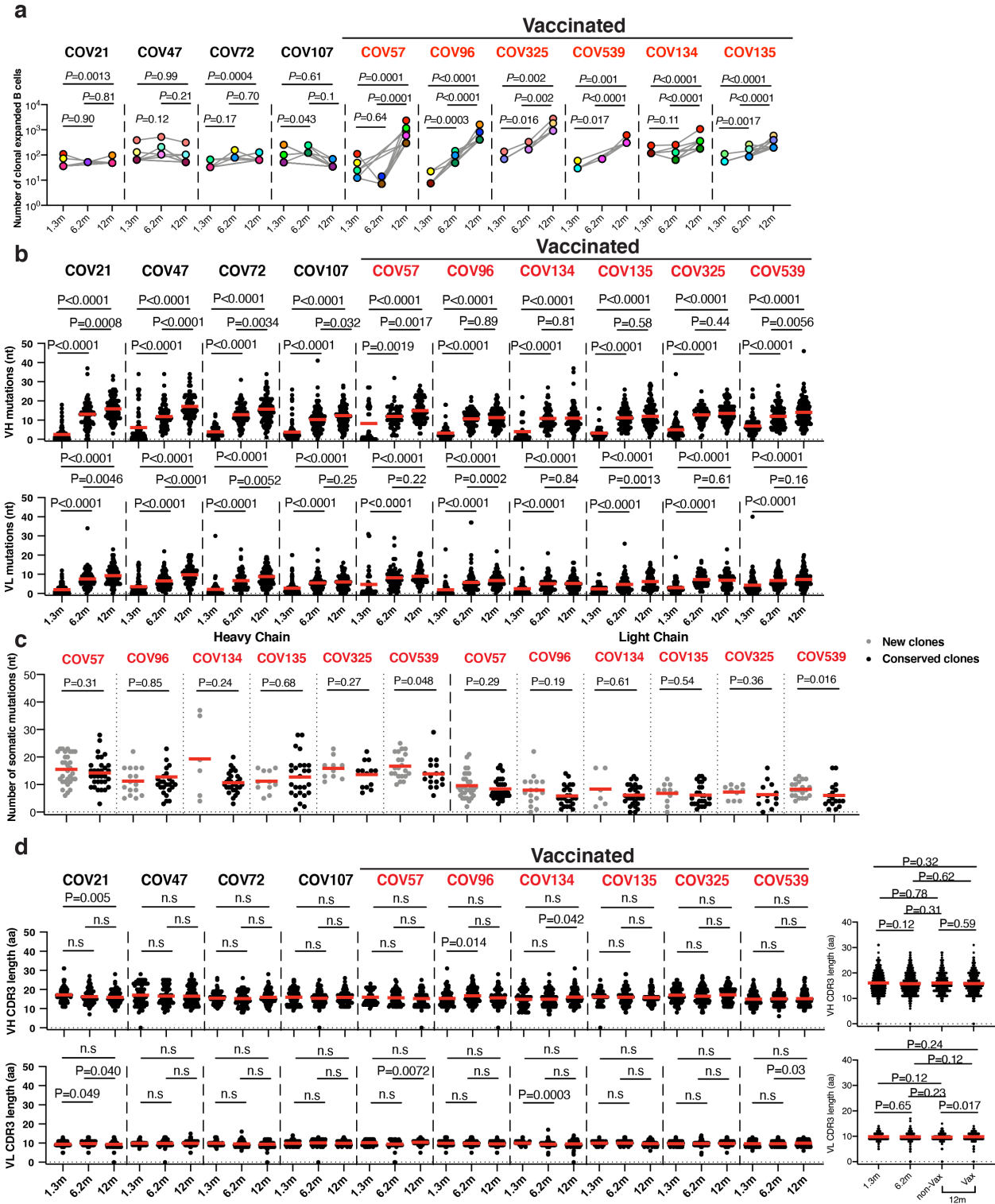
706



707

708 **Extended Data Fig. 4: Frequency distribution of human V genes.** Graph shows comparison of  
709 the frequency distributions of human V genes of anti-SARS-CoV-2 antibodies from donors at 1.3<sup>3</sup>,  
710 6.2<sup>4</sup>, 12 months after infection. **a**, Graph shows relative abundance of human IGVH genes  
711 Sequence Read Archive accession SRP010970 (green), convalescent vaccinees (blue), and  
712 convalescent non-vaccinees (orange). Statistical significance was determined by two-sided  
713 binomial test. **b and c**, same as in **a**, but showing comparison between antibodies from donors at  
714 1.3 months<sup>3</sup> (**b**), 6.2 month<sup>4</sup> (**c**), and 12 months after infection. Two-sided binomial tests with  
715 unequal variance were used to compare the frequency distributions., significant differences are  
716 denoted with stars (\*  $p < 0.05$ , \*\*  $p < 0.01$ , \*\*\*  $p < 0.001$ , \*\*\*\* =  $p < 0.0001$ ).  
717



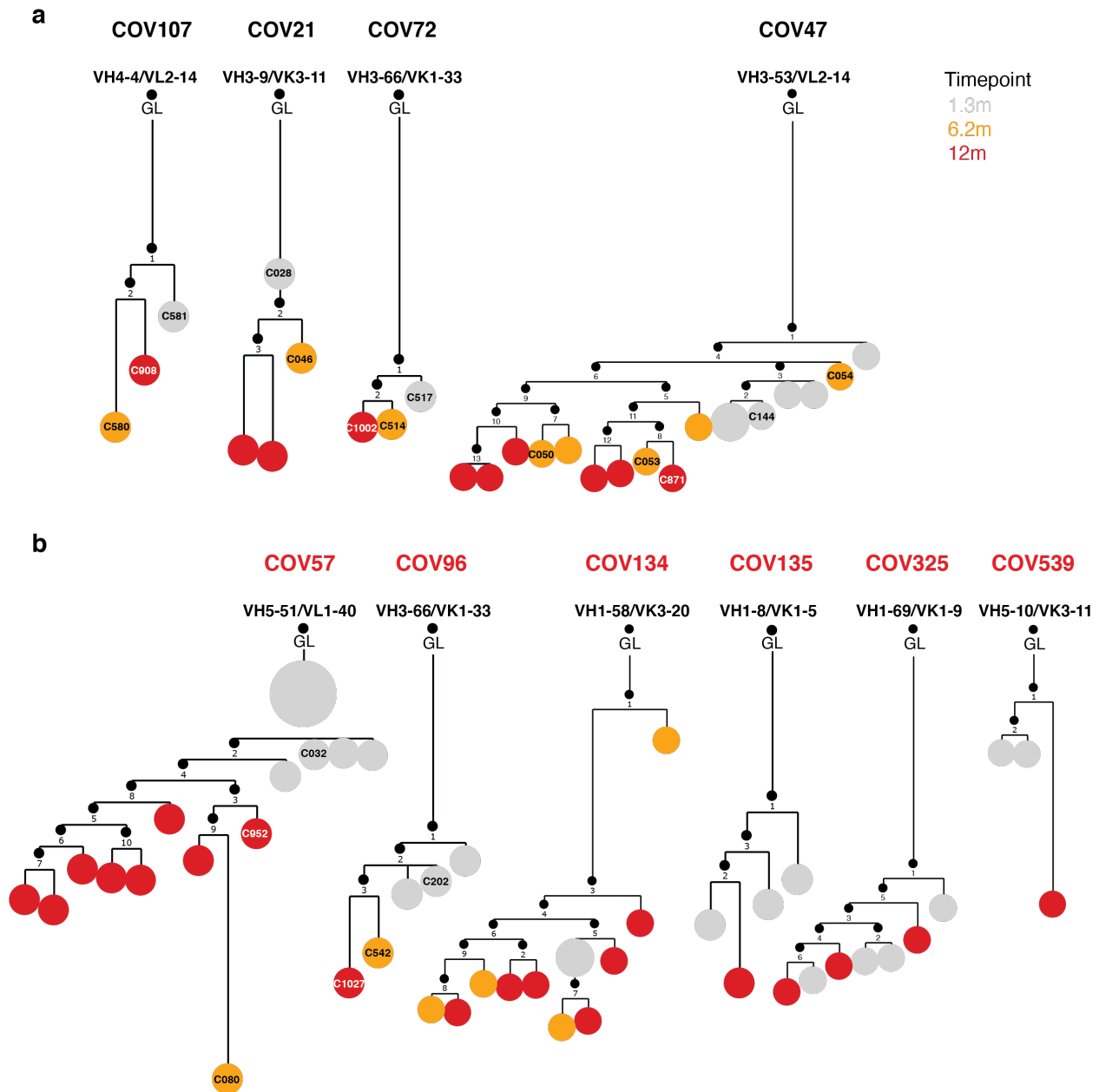


718

719

720 **Extended Data Fig. 5: Analysis of anti-RBD antibodies. a**, Number of clonally expanded B cells  
721 (per 10 million B cells) at indicated time points in 10 individuals. Colors indicate shared clones  
722 appearing at different time points. Statistical significance was determined using two-tailed  
723 Wilcoxon matched-pairs signed rank test. Vaccinees are marked in red. Statistical significance was  
724 determined using Wilcoxon matched-pairs signed rank tests. Vaccinees are marked in red. **b**.  
725 Number of somatic nucleotide mutations in the IGVH (top) and IGVL (bottom) in antibodies  
726 obtained after 1.3 or 6.2 or 12 months from the indicated individual. **c**. same as **b**, but graphs show  
727 comparison between new clones and conserved clones in 6 vaccinated convalescent individuals at  
728 12 months after infection. **d**. The amino acid length of the CDR3s at the IGVH and IGVL for each  
729 individual. Right panel shows all antibodies combined. (1.3m: n=889; 6.2m: n=975; 12m: n=1105,  
730 (non-vax: n=417; vax: n=688)). The horizontal bars indicate the mean. Statistical significance was  
731 determined using two-sided Kruskal-Wallis test with subsequent Dunn's multiple comparisons (**a**,  
732 **b** and **d**), or two-tailed Mann-Whitney U-tests (**c**).  
733

734



735

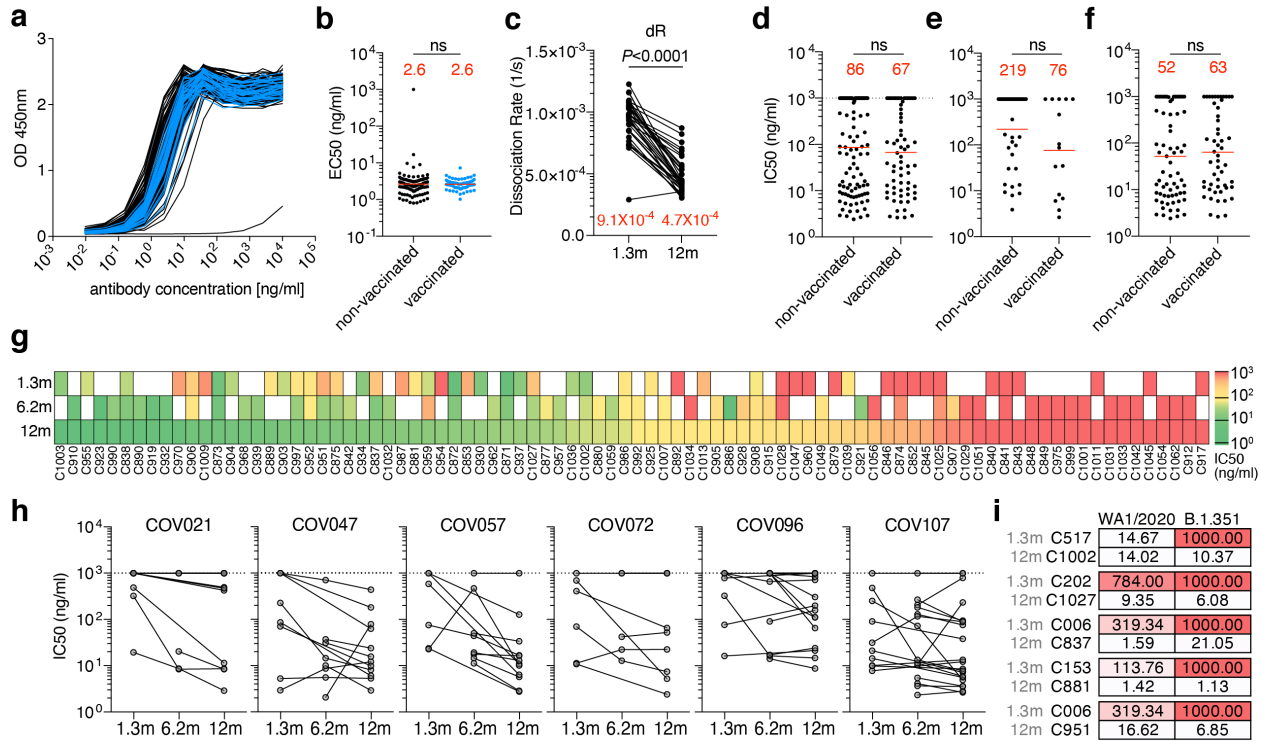
736 **Extended Data Fig. 6: Evolution of anti-SARS-CoV-2 RBD antibody clone.** Clonal evolution

737 of RBD-binding memory B cells from ten convalescent individuals, **a**, phylogenetic tree graph

738 shows clones from convalescent non-vaccinees, **b**, same as **a**, but from convalescent vaccinees.

739 Numbers refer to mutations compared to the preceding vertical node. Colors indicate timepoint;

740 grey, orange and red represent 1.3, 6 and 12 months respectively, black dots indicate inferred  
741 nodes, and size is proportional to sequence copy number; GL = germline sequence.  
742



743

744 **Extended Data Fig. 7: WT RBD binding and pseudovirus neutralization. a,b,** Binding curves

745 **(a)** and  $EC_{50}$  dot plot **(b)** of mAbs isolated from non-vaccinated (black curves and dots) and from

746 vaccinated (blue curves and dots) convalescents individuals 12 months after infection ( $p=0.74$ ). **c,**

747 Avidity (dissociation rate) measuring plasma reactivity to RBD at the 1.3- and 12-month follow-

748 up visit ( $n=33$ ). **d-f,**  $IC_{50}$  values of mAbs isolated 12 months after infection from non-vaccinated

749 and vaccinated individuals. **d** shows all 12-month antibodies irrespective of clonality, **e** shows

750 singlets only, and **f** shows only antibodies belonging to a clone or shared over time. Statistical

751 significance in **b, d-f** was determined using the two-tailed Mann-Whitney test; **c** was determined

752 using two-tailed Wilcoxon test. The geometric mean  $EC_{50}$  and  $IC_{50}$  are indicated in red. **g.** Heat

753 map shows the neutralizing activity of clonally related antibodies against wt-SARS-CoV-2 over

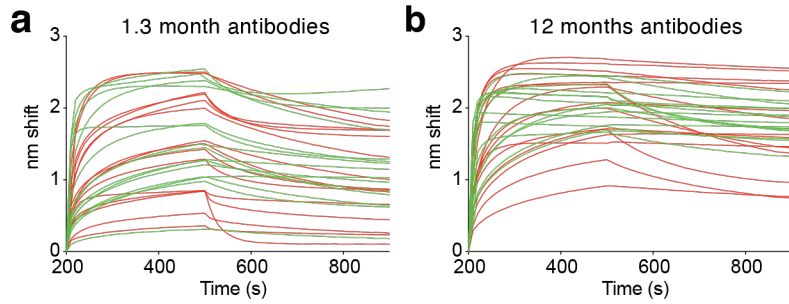
754 time. White tiles indicate no clonal relative at the respective time point. Clones are ranked from

755 left to right by the potency of the 12-month progeny antibodies which are denoted below the tiles.

756 **h**, IC<sub>50</sub> values of shared clones of mAbs cloned from B cells from the initial 1.3- and 6.2, as well  
757 as 12-month follow-up visit, divided by participant, as indicated. Lines connect clonal antibodies  
758 shared between time points. Antibodies with IC<sub>50</sub>>1000ng/ml are plotted at 1000 ng/ml in panels  
759 d-h. **i**, IC<sub>50</sub> values of 5 neutralizing antibody pairs against indicated authentic SARS-CoV-2  
760 WA1/2020 and B.1.351 viruses (n=10). Average EC<sub>50</sub> and IC<sub>50</sub> values of two independent  
761 experiments are shown.

762

763



764

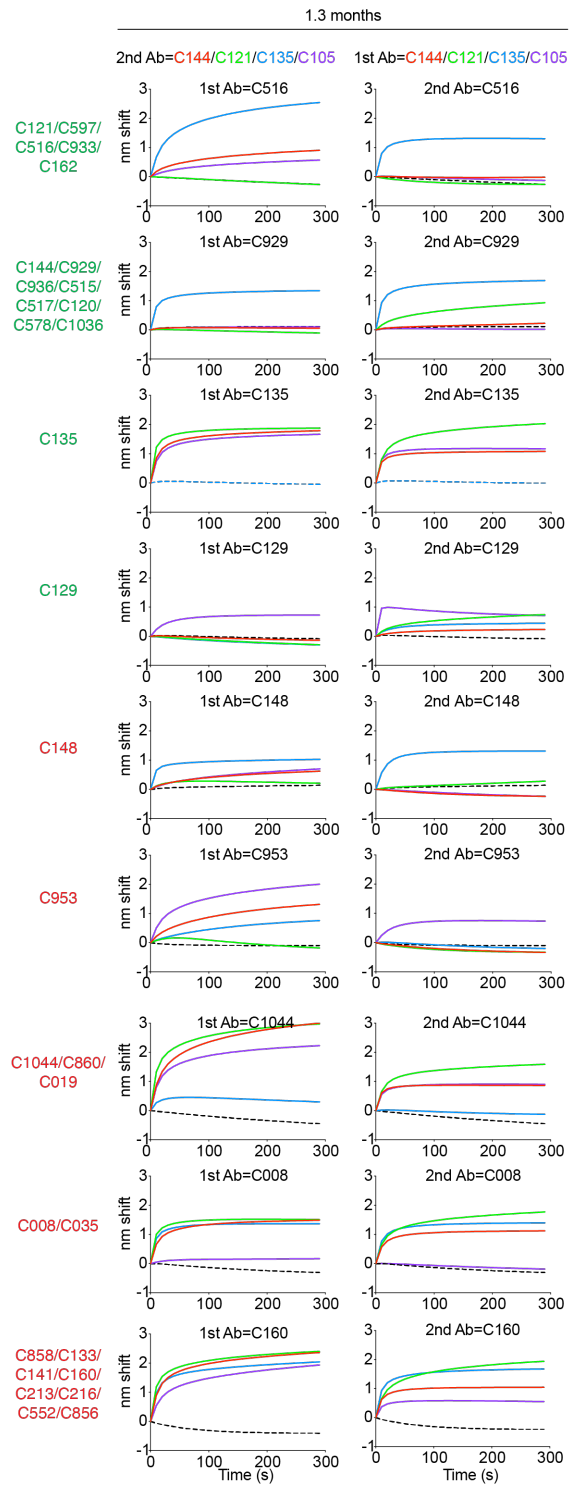
765

766 **Extended Data Fig. 8: Biolayer interferometry affinity measurements. a-b,** Graphs depict  
767 affinity measurements of neutralizing (green) and non-neutralizing (red) antibodies isolated 1.3  
768 months (**a**) or 12 months (**b**) after infection.

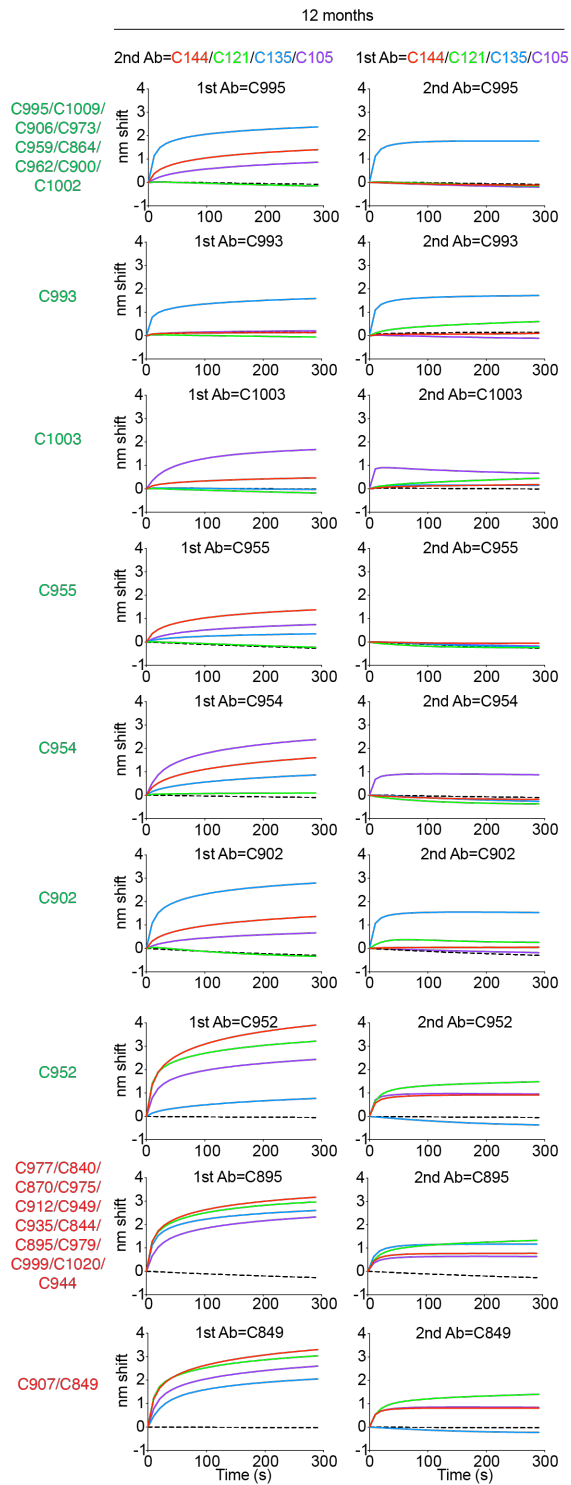
769

770

**a**



**b**



771



772 **Extended Data Fig. 9: Biolayer interferometry antibody competition experiment. a-b,** Anti-  
773 SARS-CoV-2 RBD antibodies isolated 1.3 (a) or 12 months (b) after infection were assayed for  
774 competition with structurally characterized anti-RBD antibodies by biolayer interferometry  
775 experiments as in Fig 4a. Graphs represent the binding of the second antibody (2nd Ab) to  
776 preformed first antibody (1st Ab)–RBD complexes. Dotted line denotes when 1st Ab and 2nd Ab  
777 are the same. For each antibody group identified in Fig 4c the left graphs represent the binding of  
778 the class-representative C144, C121, C135 or C105<sup>3,23</sup>(2nd Ab) to the candidate antibody (1st  
779 Ab)-RBD complex. The right graphs represent the binding of the candidate antibody (2nd Ab) to  
780 the complex of C144-RBD, C121-RBD, C135-RBD or C105-RBD (1st Ab). Antibodies belonging  
781 to the same groups are indicated to the left of the respective curves.

782

783 **Supplementary Tables**

784 **Supplementary Table 1: Cohort summary**

785 **Supplementary Table 2: Individual participant characteristics**

786 **Supplementary Table 3: Antibody sequences from patients is provided as a separate Excel**

787 **file.**

788 **Supplementary Table 4: Sequences, half maximal effective concentrations (EC50s) and**

789 **inhibitory concentrations (IC50s) of the cloned monoclonal antibodies is provided as a**

790 **separate Excel file.**

791 **Supplementary Table 5: Binding and Neutralization activity of mAbs against mutant**

792 **SARS-CoV-2 pseudoviruses.**

793 **Supplementary Table 6: Neutralization activity of mAbs against mutant SARS-CoV-2**

794 **pseudoviruses - Random potently neutralizing antibodies isolated at 1.3 and 12 months**

795 **Supplementary Table 7: Antibody affinities and neutralization - Clonal pairs isolated at 1.3**

796 **and 12 months**

797 **Supplementary Table 8: Neutralization activity of mAbs against mutant SARS-CoV-2**

798 **pseudoviruses - Clonal pairs isolated at 1.3 and 12 months.**

799

800 **Reference:**

- 801 1 Davies, N. G. *et al.* Estimated transmissibility and impact of SARS-CoV-2 lineage B.1.1.7  
802 in England. *Science* **372**, doi:10.1126/science.abg3055 (2021).
- 803 2 Wang, Z. *et al.* mRNA vaccine-elicited antibodies to SARS-CoV-2 and circulating variants.  
804 *Nature* **592**, 616-622, doi:10.1038/s41586-021-03324-6 (2021).
- 805 3 Robbiani, D. F. *et al.* Convergent antibody responses to SARS-CoV-2 in convalescent  
806 individuals. *Nature* **584**, 437-442, doi:10.1038/s41586-020-2456-9 (2020).
- 807 4 Gaebler, C. *et al.* Evolution of antibody immunity to SARS-CoV-2. *Nature* **591**, 639-644,  
808 doi:10.1038/s41586-021-03207-w (2021).
- 809 5 Goel, R. R. *et al.* Distinct antibody and memory B cell responses in SARS-CoV-2 naive and  
810 recovered individuals following mRNA vaccination. *Sci Immunol* **6**,  
811 doi:10.1126/sciimmunol.abi6950 (2021).
- 812 6 Saadat, S. *et al.* Binding and Neutralization Antibody Titers After a Single Vaccine Dose in  
813 Health Care Workers Previously Infected With SARS-CoV-2. *JAMA* **325**, 1467-1469,  
814 doi:10.1001/jama.2021.3341 (2021).
- 815 7 Krammer, F. *et al.* Antibody Responses in Seropositive Persons after a Single Dose of  
816 SARS-CoV-2 mRNA Vaccine. *N Engl J Med* **384**, 1372-1374, doi:10.1056/NEJMc2101667  
817 (2021).
- 818 8 Reynolds, C. J. *et al.* Prior SARS-CoV-2 infection rescues B and T cell responses to  
819 variants after first vaccine dose. *Science*, doi:10.1126/science.abh1282 (2021).
- 820 9 Muecksch, F. *et al.* Development of potency, breadth and resilience to viral escape  
821 mutations in SARS-CoV-2 neutralizing antibodies. *bioRxiv*,  
822 doi:10.1101/2021.03.07.434227 (2021).
- 823 10 Brouwer, P. J. M. *et al.* Potent neutralizing antibodies from COVID-19 patients define  
824 multiple targets of vulnerability. *Science* **369**, 643-650, doi:10.1126/science.abc5902  
825 (2020).
- 826 11 Cao, Y. *et al.* Potent Neutralizing Antibodies against SARS-CoV-2 Identified by High-  
827 Throughput Single-Cell Sequencing of Convalescent Patients' B Cells. *Cell* **182**, 73-84 e16,  
828 doi:10.1016/j.cell.2020.05.025 (2020).
- 829 12 Ju, B. *et al.* Human neutralizing antibodies elicited by SARS-CoV-2 infection. *Nature* **584**,  
830 115-119, doi:10.1038/s41586-020-2380-z (2020).
- 831 13 Schmidt, F. *et al.* Measuring SARS-CoV-2 neutralizing antibody activity using  
832 pseudotyped and chimeric viruses. *J Exp Med* **217**, doi:10.1084/jem.20201181 (2020).
- 833 14 Tegally, H. *et al.* Detection of a SARS-CoV-2 variant of concern in South Africa. *Nature*  
834 **592**, 438-443, doi:10.1038/s41586-021-03402-9 (2021).
- 835 15 West, A. P. *et al.* Detection and characterization of the SARS-CoV-2 lineage B.1.526 in  
836 New York. *bioRxiv*, 2021.2002.2014.431043, doi:10.1101/2021.02.14.431043 (2021).
- 837 16 Inoue, T. *et al.* Exit from germinal center to become quiescent memory B cells depends  
838 on metabolic reprogramming and provision of a survival signal. *J Exp Med* **218**,  
839 doi:10.1084/jem.20200866 (2021).
- 840 17 Viant, C. *et al.* Antibody Affinity Shapes the Choice between Memory and Germinal  
841 Center B Cell Fates. *Cell* **183**, 1298-1311 e1211, doi:10.1016/j.cell.2020.09.063 (2020).

- 842 18 Rogers, T. F. *et al.* Isolation of potent SARS-CoV-2 neutralizing antibodies and protection  
843 from disease in a small animal model. *Science* **369**, 956-963,  
844 doi:10.1126/science.abc7520 (2020).
- 845 19 Kreer, C. *et al.* Longitudinal Isolation of Potent Near-Germline SARS-CoV-2-Neutralizing  
846 Antibodies from COVID-19 Patients. *Cell* **182**, 1663-1673, doi:10.1016/j.cell.2020.08.046  
847 (2020).
- 848 20 Stamatatos, L. *et al.* mRNA vaccination boosts cross-variant neutralizing antibodies  
849 elicited by SARS-CoV-2 infection. *Science*, doi:10.1126/science.abg9175 (2021).
- 850 21 Sokal, A. *et al.* Maturation and persistence of the anti-SARS-CoV-2 memory B cell  
851 response. *Cell* **184**, 1201-1213 e1214, doi:10.1016/j.cell.2021.01.050 (2021).
- 852 22 Sakharkar, M. *et al.* Prolonged evolution of the human B cell response to SARS-CoV-2  
853 infection. *Sci Immunol* **6**, doi:10.1126/sciimmunol.abg6916 (2021).
- 854 23 Barnes, C. O. *et al.* SARS-CoV-2 neutralizing antibody structures inform therapeutic  
855 strategies. *Nature* **588**, 682-687, doi:10.1038/s41586-020-2852-1 (2020).
- 856 24 Hoffmann, M. *et al.* SARS-CoV-2 Cell Entry Depends on ACE2 and TMPRSS2 and Is  
857 Blocked by a Clinically Proven Protease Inhibitor. *Cell* **181**, 271-280 e278,  
858 doi:10.1016/j.cell.2020.02.052 (2020).
- 859 25 Greaney, A. J. *et al.* Mutational escape from the polyclonal antibody response to SARS-  
860 CoV-2 infection is largely shaped by a single class of antibodies. *bioRxiv*,  
861 doi:10.1101/2021.03.17.435863 (2021).
- 862 26 Weisblum, Y. *et al.* Escape from neutralizing antibodies by SARS-CoV-2 spike protein  
863 variants. *Elife* **9**, doi:10.7554/eLife.61312 (2020).
- 864 27 Elsner, R. A. & Shlomchik, M. J. Germinal Center and Extrafollicular B Cell Responses in  
865 Vaccination, Immunity, and Autoimmunity. *Immunity* **53**, 1136-1150,  
866 doi:10.1016/j.immuni.2020.11.006 (2020).
- 867 28 Lau, A. W. & Brink, R. Selection in the germinal center. *Curr Opin Immunol* **63**, 29-34,  
868 doi:10.1016/j.coi.2019.11.001 (2020).
- 869 29 Victora, G. D. & Nussenzweig, M. C. Germinal centers. *Annu Rev Immunol* **30**, 429-457,  
870 doi:10.1146/annurev-immunol-020711-075032 (2012).
- 871 30 Inoue, T., Moran, I., Shinnakasu, R., Phan, T. G. & Kurosaki, T. Generation of memory B  
872 cells and their reactivation. *Immunol Rev* **283**, 138-149, doi:10.1111/imr.12640 (2018).
- 873 31 Taylor, J. J., Pape, K. A., Steach, H. R. & Jenkins, M. K. Humoral immunity. Apoptosis and  
874 antigen affinity limit effector cell differentiation of a single naive B cell. *Science* **347**,  
875 784-787, doi:10.1126/science.aaa1342 (2015).
- 876 32 McKean, D. *et al.* Generation of antibody diversity in the immune response of BALB/c  
877 mice to influenza virus hemagglutinin. *Proc Natl Acad Sci U S A* **81**, 3180-3184,  
878 doi:10.1073/pnas.81.10.3180 (1984).
- 879 33 Petersen, M. S. *et al.* SARS-CoV-2 natural antibody response persists up to 12 months in  
880 a nationwide study from the Faroe Islands. *medRxiv*, 2021.2004.2019.21255720,  
881 doi:10.1101/2021.04.19.21255720 (2021).
- 882 34 Li, C. *et al.* Twelve-month specific IgG response to SARS-CoV-2 receptor-binding domain  
883 among COVID-19 convalescent plasma donors in Wuhan. *bioRxiv*,  
884 2021.2004.2005.437224, doi:10.1101/2021.04.05.437224 (2021).

- 885 35 Turner, J. *et al.* SARS-CoV-2 mRNA vaccines induce a robust germinal centre reaction in  
886 humans. *Research Square*, doi:<https://www.researchsquare.com/article/rs-310773/v1>  
887 (2021).
- 888 36 Greaney, A. J. *et al.* The SARS-CoV-2 mRNA-1273 vaccine elicits more RBD-focused  
889 neutralization, but with broader antibody binding within the RBD. *bioRxiv*,  
890 doi:10.1101/2021.04.14.439844 (2021).
- 891 37 Wang, Z. *et al.* Enhanced SARS-CoV-2 neutralization by dimeric IgA. *Sci Transl Med* **13**,  
892 doi:10.1126/scitranslmed.abf1555 (2021).
- 893 38 Schoof, M. *et al.* An ultrapotent synthetic nanobody neutralizes SARS-CoV-2 by  
894 stabilizing inactive Spike. *Science* **370**, 1473-1479, doi:10.1126/science.abe3255 (2020).
- 895 39 De Gasparo, R. *et al.* Bispecific IgG neutralizes SARS-CoV-2 variants and prevents escape  
896 in mice. *Nature*, doi:10.1038/s41586-021-03461-y (2021).
- 897 40 Xu, J. *et al.* Multimeric nanobodies from camelid engineered mice and llamas potently  
898 neutralize SARS-CoV-2 variants. *bioRxiv*, doi:10.1101/2021.03.04.433768 (2021).
- 899 41 Wu, F. *et al.* A new coronavirus associated with human respiratory disease in China.  
900 *Nature* **579**, 265-269, doi:10.1038/s41586-020-2008-3 (2020).
- 901 42 Chomczynski, P. & Sacchi, N. Single-step method of RNA isolation by acid guanidinium  
902 thiocyanate-phenol-chloroform extraction. *Analytical biochemistry* **162**, 156-159,  
903 doi:10.1006/abio.1987.9999 (1987).
- 904 43 DeAngelis, M. M., Wang, D. G. & Hawkins, T. L. Solid-phase reversible immobilization for  
905 the isolation of PCR products. *Nucleic Acids Res* **23**, 4742-4743,  
906 doi:10.1093/nar/23.22.4742 (1995).
- 907 44 Grifoni, A. *et al.* Targets of T Cell Responses to SARS-CoV-2 Coronavirus in Humans with  
908 COVID-19 Disease and Unexposed Individuals. *Cell* **181**, 1489-1501 e1415,  
909 doi:10.1016/j.cell.2020.05.015 (2020).
- 910 45 Amanat, F. *et al.* A serological assay to detect SARS-CoV-2 seroconversion in humans.  
911 *Nat Med* **26**, 1033-1036, doi:10.1038/s41591-020-0913-5 (2020).
- 912 46 Barnes, C. O. *et al.* Structures of Human Antibodies Bound to SARS-CoV-2 Spike Reveal  
913 Common Epitopes and Recurrent Features of Antibodies. *Cell* **182**, 828-842 e816,  
914 doi:10.1016/j.cell.2020.06.025 (2020).
- 915 47 Racine-Brzostek, S. E. *et al.* TOP-Plus is a Versatile Biosensor Platform for Monitoring  
916 SARS-CoV-2 Antibody Durability. *Clin Chem*, doi:10.1093/clinchem/hvab069 (2021).
- 917 48 Gupta, N. T. *et al.* Change-O: a toolkit for analyzing large-scale B cell immunoglobulin  
918 repertoire sequencing data. *Bioinformatics (Oxford, England)* **31**, 3356-3358,  
919 doi:10.1093/bioinformatics/btv359 (2015).
- 920 49 Soto, C. *et al.* High frequency of shared clonotypes in human B cell receptor repertoires.  
921 *Nature* **566**, 398-402, doi:10.1038/s41586-019-0934-8 (2019).
- 922 50 Guo, Y., Chen, K., Kwong, P. D., Shapiro, L. & Sheng, Z. cAb-Rep: A Database of Curated  
923 Antibody Repertoires for Exploring Antibody Diversity and Predicting Antibody  
924 Prevalence. *Front Immunol* **10**, 2365, doi:10.3389/fimmu.2019.02365 (2019).
- 925 51 Abascal, F., Zardoya, R. & Telford, M. J. TranslatorX: multiple alignment of nucleotide  
926 sequences guided by amino acid translations. *Nucleic Acids Res* **38**, W7-13,  
927 doi:10.1093/nar/gkq291 (2010).

928 52 Lefranc, M. P. IMGT, the International ImMunoGeneTics Information System. *Cold*  
929 *Spring Harb Protoc* **2011**, 595-603, doi:10.1101/pdb.top115 (2011).  
930 53 DeWitt, W. S., 3rd, Mesin, L., Victora, G. D., Minin, V. N. & Matsen, F. A. t. Using  
931 Genotype Abundance to Improve Phylogenetic Inference. *Mol Biol Evol* **35**, 1253-1265,  
932 doi:10.1093/molbev/msy020 (2018).  
933